LU-TP 21-49
March 2022

Matter-streams as sources of the Kerr metric

Julian Boy

Department of Astronomy and Theoretical Physics, Lund University

Master thesis supervised by Johan Bijnens

LUND
UNIVERSITY

Abstract

An introduction to the thin-shell formalism and distributional approach to General Relativity is provided. The formalism is utilized to investigate possible distributions of matter that can act as a source to the Kerr metric. As a precursor to a collapsing surface, we recall how two counter-rotating streams of matter can be constructed to act as a source which we examine in two cases: one for a frame where the surface energy-momentum tensor is diagonal and one where the streams follow geodesics. No fully time-dependent and analytical solutions have previously been found that act as a collapsing source of the Kerr metric. We show that, for an adiabatic collapse up to first order, the surface energy-momentum tensor is incompatible with geodesic streams of matter and that diagonalizing it results in complex parameters for gravitational collapse.

Populärvetenskaplig beskrivning

Sedan den *Allmänna relativitetsteorin* publicerades år 1916 har det bedrivits mängder av forskning inom detta forskningsområde. De matematiska redskap som togs fram gjorde det möjligt att förstå den inre strukturen hos universum: från Big Bang, krökning av rum och tid till svarta hål och maskhål, så har allmänn relativitetsteori ökat vår förståelse av Universum avsevärt.

Kanske den viktigaste tillämpningen av allmän relativitetsteori gäller solens inre struktur, men även dess påverkan på planeternas rörelse. Genom att förklara stjärnors påverkan på rumtiden utvecklades matematiska redskap som möjliggjorde, för första gången någonsin, en förståelse av kanske de mest bisarra objekten i universum: svarta hål.

Karl Schwarzschild publicerade den första kompletta bilden av hur rumtiden böjs kring massiva objekt, bara några månader efter Einsteins approximation av samma fenomen. Schwarzschild konstruerade en *metrik*; ett matematiskt redskap för att "mäta" krökningen kring massiva kroppar. Man insåg bara något år senare att metriken faktiskt beskrev ett svart hål; materia komprimerad till en oändligt liten punkt med oändligt hög densitet. Ytterligare sju år passerade innan George Birkhoff konstaterade, med ett matematiskt teorem, att objekt som solen - till en viss grad - gav upphov till en krökt rumtid som kunde beskrivas med hjälp av Schwarzschilds metrik.

Denna framgång medförde dock en oro: ingenting i Universum är stillastående, och man förstod tidigt att Schwarzschilds metrik bara var en ungefärlig beskrivning av verkligheten. Det kliade i teoretikers fingrar i ungefär fyrtio år innan Roy Kerr publicerade sin metrik, som beskriver hur rumtiden böjs kring roterande svarta hål. Dessvärre finns inget teorem som säkerställer att vilken roterande massiv kropp som helst ger upphov till den. Därför pågår det en stor mängd forskning för att ta fram så kallade "källor" till Kerrs metrik, för att se vilka typer av massiva kroppar som kan ge upphov till den - är solen en av dem?

I denna uppsats är målet att undersöka stabila källor till Kerrs metrik, men även de fall där de kollapsar likt en roterande stjärna som exploderar i en supernova. Vi antar att källorna består av två roterande strömmar av materia och undersöker de egenskaper som uppkommer som en konsekvens av Einsteins fältekvationer.

Att undersöka en källas kollaps visade sig vara väldigt svårt och i denna uppsats begränsar vi oss till den ursprungliga utvecklingen i början av en kollaps – och visar att det inte finns någon lösning som tyder på en långsam och gradvis ursprunglig kollaps.

Contents

1 Introduction

Not long after the publication of the landmark theory *General Relativity* (GR) in 1916 [1], a solution for static, non-rotating black holes was found by Karl Schwarzschild [2]. For the first time, all of the significant celestial movements could be explained, including the precession of Mercury's orbit. This solution of Einstein's field equations, called the *Schwarzschild metric*, describes the curvature of spacetime around massive objects. An interior solution was later found in 1939, providing the first general relativistic framework of the collapse of stars [3].

The Schwarzschild metric proved to be very useful, but it was missing a key component: rotation. Everything we see in the universe moves somehow, and a rotation around the axis is more of a fact than circumstance as a consequence of the conservation of angular momentum. A metric incorporating a rotation about the axis for gravitationally collapsed objects was introduced in 1963 by Roy Kerr and is a beloved mathematical object by physicists [4]. It describes the curvature of spacetime (and hence the movement of particles) around a rotating black hole. It predicted several exciting phenomena: a complete description of frame-dragging (previously only known in limiting cases [5]), ring-singularities, and gave rise to questions such as naked singularities and hyper-efficient energy resources [6]. The hope for an interior solution that can act as a source of the Kerr metric built up, but no analytical solutions have been found. An interior solution is of interest because one of the most extreme objects in the universe, neutron stars, rotates. It is unknown how much extreme rotations affect the interior of such objects.

Various approaches in the hunt for an interior solution have come to light [7, 8, 9], but this thesis will utilize the thin-shell formalism of general relativity, specifically restricting ourselves to a part of a given spacetime. Loosely speaking, we cut out a part of it, and say that the resulting spacetime - a "surface" - has a new so-called induced metric with a discontinuous normal derivative defined on it when crossing the surface. We cut out this surface through the gluing of two spacetime metrics, and by subsequently using a distributional approach of the Einstein field equations explained below, we find the physical properties of it [10].

We introduce, in section 2, the coordinates used along with specific observers and the concept of ergoregions. Following that, an introduction to the thin-shell formalism and Israel Junction conditions will be provided in section 3, and important energy conditions used together with this formalism are presented in section 4. Derivation of physical properties of gravitating surfaces, or, "disks", such as densities and pressure for different physical configurations of matter, will be made in sections 5-7. This will be done by utilizing a discrete distribution of the metric tensor - where the intermediate part (at the cut-out region) will be interpreted as the surface mentioned - and subsequently, collect all of the singular parts that arise in the Ricci tensor and its corresponding scalar. Inserting these results into Einstein's field equations will lead to a discrete distribution of the energy-momentum tensor, requiring an additional part – the energy-density and pressure of the surface. We

will reproduce results of [8] by deriving two counter-rotating vectors that decompose the resulting energy-momentum tensor and show their densities and pressures. We will see that this can be done in two cases: one where the vectors diagonalize the energy-momentum tensor of the surface, and one case where they are assumed to follow geodesics [9]. In section 7, however, we expand upon the results of [9] to include gravitational collapse to see if one can find vectors that are co-moving with the collapsing surface that satisfies the geodesic equation. This is done by imposing a time dependence on the surface of the cut-out region and taking a first-order approximation. Finally, section 8 summarizes the results and concludes that no first-order perturbations of the disk to simulate gravitational collapse exist.

2 Coordinates and observers with zero angular momentum

The choice of coordinate systems in General Relativity is an arbitrary matter; they are mainly chosen for specific reasons, such as getting rid of coordinate singularities or rewriting metrics for symmetries to become apparent (such as spherical symmetries.)

A vector basis is often defined to use as a tool for describing physical quantities such as four-velocities and the energy-momentum tensor (EMT) in different frames of reference, such as stationary ones. The reason for doing this is because tensorial quantities can be better understood if viewed through the eyes of specific observers, such as those with zero angular momentum (but a non-zero angular velocity) abbreviated ZAMO, or those who observe a diagonal form of the EMT, here called FIOs, or, $\phi-$isotropic frames [11, 12].

In this section, we define the coordinates used for an axially symmetric metric (specifically the Kerr metric) throughout this thesis, and how they relate to the familiar Boyer-Lindqvist (BL) coordinates [13]. We will also demonstrate the value of finding ZAMOs by deriving an expression for the angular velocity of rotating streams of matter as observed by the ZAMO.

The Kerr metric is expressed in BL-coordinates (t, r, θ, ϕ), using natural units ($c = G = 1$), through

$$ds^2 = g_{tt}dt^2 + g_{rr}dr^2 + 2g_{t\phi}dtd\phi + g_{\phi\phi}d\phi^2 + g_{\theta\theta}d\theta^2, \tag{1}$$

where

$$g_{\mu\nu} = \begin{pmatrix} -\left(1 - \frac{2Mr}{\Sigma}\right) & 0 & 0 & -\frac{2Mra\sin^2(\theta)}{\Sigma} \\ 0 & \frac{\Sigma}{\Delta} & 0 & 0 \\ 0 & 0 & \Sigma & 0 \\ -\frac{2Mra\sin^2(\theta)}{\Sigma} & 0 & 0 & \left(r^2 + a^2 + \frac{2Mra^2}{\Sigma}\sin^2(\theta)\right)\sin^2(\theta) \end{pmatrix}. \tag{2}$$

The parameter $a = J/M$ signifies the angular momentum J per unit mass M, and Σ and

Δ are expressed as

$$\Sigma = r^2 + a^2\cos(\theta)^2 \quad \Delta = r^2 - 2Mr + a^2. \tag{3}$$

2.1 Weyl-Papapetrou coordinates

The Weyl-Papapetrou (WP)-coordinates (t, ϕ, ρ, z) are used to put the Kerr metric into a general axially symmetric form [14, 15, 16]. The Kerr metric is then expressed as

$$ds^2 = \frac{h}{f}\left(d\rho^2 + dz^2\right) + \frac{\rho^2}{f}d\phi^2 - f\left(dt + Ad\phi\right)^2, \tag{4}$$

in which h, f and A are functions of ρ and z. Here, the coordinates ρ and z are related to the BL-coordinates as

$$\begin{aligned} \rho &= \frac{\delta\sin(\theta)}{Mp}\sqrt{r^2 - 2Mr - a^2}, \\ z &= \frac{\delta(r-M)\cos(\theta)}{Mp}, \end{aligned} \tag{5}$$

where M is the mass of the source. The parameters δ and p are related to the angular rotation parameter a in the case of a Kerr black hole as

$$\delta = Mp, \quad p^2 = \frac{1 - a^2/M^2}{\kappa}. \tag{6}$$

Note that δ is defined here (even though it cancels in Eq.(5) in the case for a Kerr black hole) due to its importance later on. κ signifies the shape of our coordinate system; $\kappa = 1$ is the prolate kind and $\kappa = -1$ the oblate kind. A prolate set of coordinates (for a sphere) means that it is squeezed in the direction of the polar coordinate, in contrast to the oblate case, where it is stretched. In this thesis, we will only concern ourselves with the prolate case, as we restrict ourselves to be outside the source's horizon. Further on, for brevity, we will introduce a new parameter $q = a/M$, which will be chosen to be 0.8 to reproduce results of [9]. For $\pi/2 \leq \theta \leq \pi$ and $M = 1$, the relation between r and z along with r and ρ can be seen in figure 1.

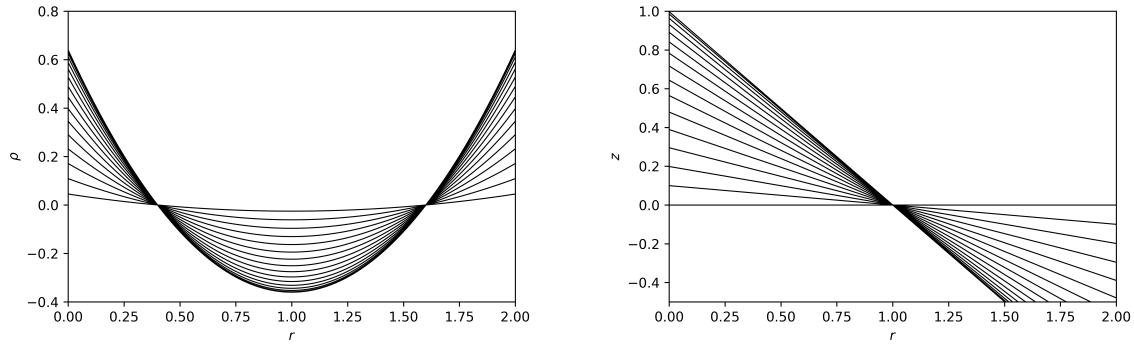

(a) Coordinate ρ as a function of the radius r. (b) Coordinate z as a function of the radius r.

Figure 1: The WP-coordinates in relation to the BL-coordinates for $\pi/2 \leq \theta \leq \pi$ and $q = 0.8$. The lines close to zero for all r corresponds to $\theta = \pi/2$.

This thesis will consider only part of the spacetime defined by the metric to construct a *disk* explained more in detail later. In other words, we will cut out part of the spacetime as illustrated in figure 2.

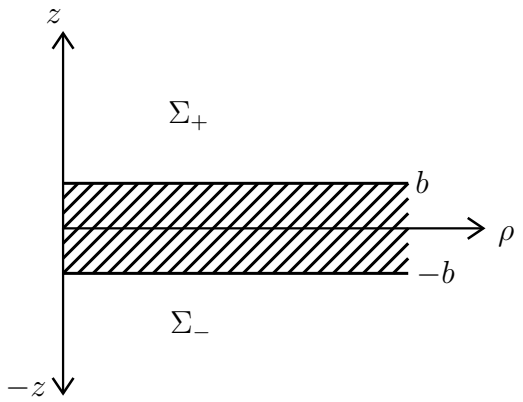

Figure 2: The cut-out region. An infinitely thin shell bounded by b and $-b$ is infinitely wide in ρ.

The part we cut out and use for our calculations depend heavily on the value of b. We can visualize the case for constant values of $z = b$ intuitively in figure 3, where they are shown to hover above the source's center.

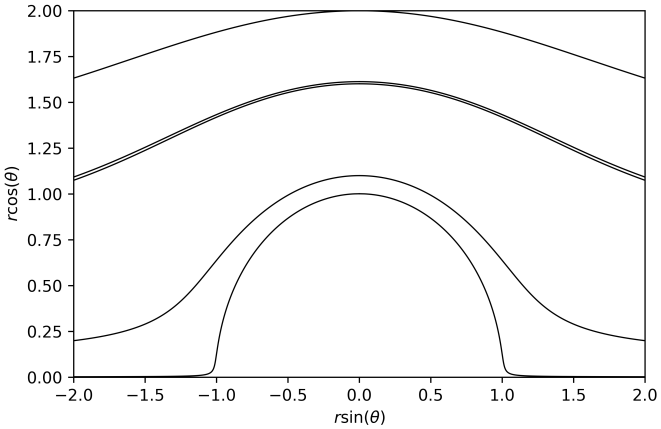

Figure 3: The lines are (from bottom up) regions at constant $b = [0.001, 0.1, 0.6013, 0.613, 1]$, shown in the BL-coordinates r and θ.

The metric functions are quite cumbersome in the WP-coordinates directly, so we introduce a new set of (spheroidal) coordinates (x, y) related to (ρ, z) by

$$\rho = \delta\sqrt{(x^2 - \kappa)(1 - y^2)},\ z = \delta xy, \tag{7}$$

where x, y are related to the BL-coordinates by $x = (r/M - 1)/p$ and $y = \cos(\theta)$. These coordinates can be used to express the metric functions:

$$\begin{aligned} f &= \frac{p^2x^2 + q^2y^2 - 1}{(px+1)^2 + q^2y^2}, \\ h &= \frac{p^2x^2 + q^2y^2 - 1}{p^2\left(-\kappa\, y^2 + x^2\right)}, \\ A &= \frac{2Mq\left(-y^2+1\right)(px+1)}{p^2x^2 + q^2y^2 - 1}. \end{aligned} \tag{8}$$

In this thesis, most quantities will be plotted against the so-called *proper circumferential radius*, defined as $R = \sqrt{g_{\phi\phi}}$. In Minkowski spacetime, we have $R = r\sin(\theta)$, which is the projection of the radius onto the x, y-plane (in cartesian coordinates). When integrated over the angle $0 \leq \phi \leq 2\pi$, it results in the circumference of radius R. However, in the Kerr metric, $R = 0$ does not imply the center of a given source but rather its horizon. The relation between the BL-coordinate r and the circumferential radius R is shown in figure 4.

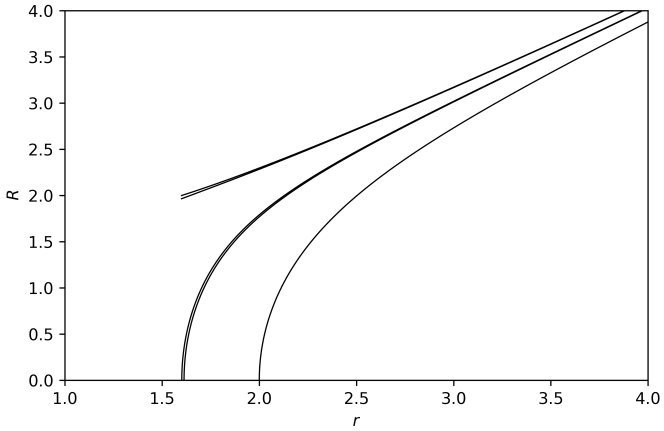

Figure 4: The proper circumferential radius in proportion to the BL-coordinate r evaluated at constant values of $z = b = [0.001, 0.1, 0.6013, 0.613, 1]$.

Note that this is for constant values of z, which does not imply constant values of θ. In fact, θ changes according to

$$\theta = \arccos\left(\frac{b}{\delta}\frac{pM}{r-M}\right), \tag{9}$$

which is shown in figure 5.

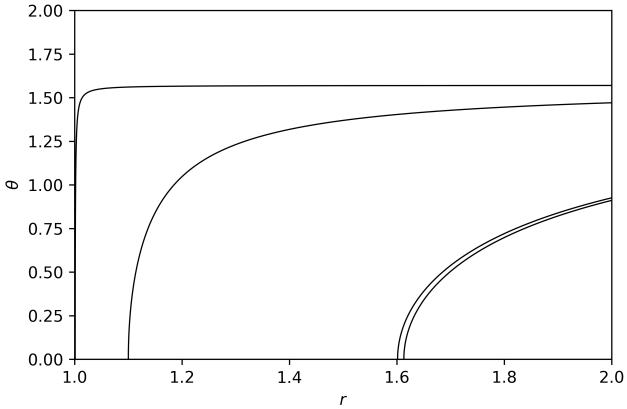

Figure 5: How the angle θ changes (from left to right) with constant $z = b = [0.001, 0.1, 0.6013, 0.613, 1]$ as we move away from the center.

2.2 Ergoregion-producing disks

As we shall see later, we will plot physical quantities for some constant value of $z = b$. Some of these disks will produce an ergoregion - a region in the Kerr metric where no stationary

frames exist - and others will not, since, as seen in figure 3, a larger value of b moves away from the source such that the cut-out region does not overlap with the ergoregion. The upper bound b_{max} will be derived here, and the lower bound will be determined later by a physical argument related to the requirement that the source has a positive energy density. We can find these constraints by noting that the ergoregion only exists a small distance from the center of the source r_{Ergo} in accordance with Eq.(10).

For $M = 1$, we know that the ergoregion exists at a radial distance from the center according to

$$r_{Ergo} = 1 + \sqrt{1 - q^2 y^2}. \tag{10}$$

For a constant value of $z = b_{max}$, we also have

$$r_{Ergo} = p\frac{b_{max}}{\delta y} + 1. \tag{11}$$

Since $y = \cos(\theta)$ we know that $-1 \leq y \leq 1$, and so we can put Eq.(10) and Eq.(11) together and solve for b

$$b_{max} \leq \frac{\delta y}{p}\sqrt{1 - q^2 y^2}. \tag{12}$$

Using $q = 0.8$, we plot the relation between b_{max} and y in figure 6.

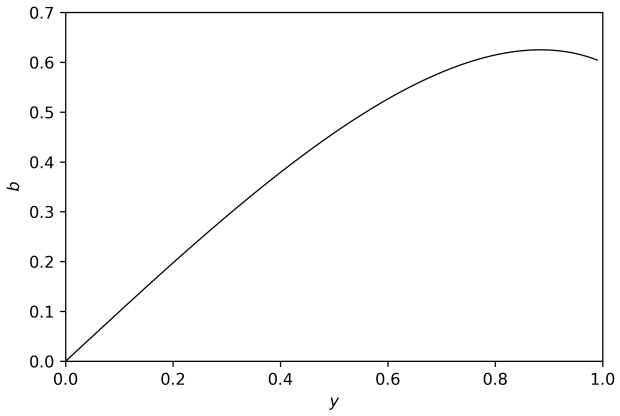

Figure 6: The values of b that can produce an ergoregion. It shows that the maximal value of b is $b_{max} \approx 0.625$.

Hence we can conclude that, for $q = 0.8$, a maximum value of $b = b_{max} \approx 0.625$. We will plot quantities for larger values than this, but they will not produce any ergoregion for $q = 0.8$.

2.3 ZAMO and LNRF

The ZAMO is an observer in the presence of a defined metric (the Kerr metric). Since frame-dragging is present as seen through the coupling of dt and $d\phi$ in Eq.(1), we expect the ZAMO to have some non-zero angular velocity even if it has zero angular momentum. The immediate goal here is to derive this frame and relate physical quantities to it - the frame is valuable for a very good reason. Normally, it is desired to observe quantities from a stationary frame. However, the ergoregion prevents stationary frames from occurring as previously mentioned, as it would require an observer very far away to move with a speed faster than light to observe them as such. Therefore, the ZAMO is a frame which can be compared to a stationary frame as it has no angular momentum.

To start, we observe the constants of motion C_α. The metric is invariant under $\phi-$ and t translations. We therefore obtain two equations of motion for the constants C_t and C_ϕ

$$\begin{aligned} \frac{dt}{d\tau} &= \frac{f^2A^2 - \rho^2}{\rho^2 f} C_t - \frac{Af}{\rho^2} C_\phi, \\ \frac{d\phi}{d\tau} &= \frac{f}{\rho^2} \left(C_\phi - C_t A \right), \end{aligned} \tag{13}$$

in which $C_t \propto E$ (energy) and $C_\phi \propto L$ (angular momentum) of the ZAMO. If we take the quotient of the second and first equation in (13), we get the angular velocity of a particle moving around the source. If the angular momentum is set to zero, we obtain

$$\frac{d\phi}{dt} = \omega = \frac{f^2 A}{\rho^2 - f^2 A^2} = -\frac{g_{t\phi}}{g_{\phi\phi}}. \tag{14}$$

This is the angular velocity of the ZAMO.

It is beneficial to describe the angular velocity relative to a locally non-rotating frame (LNRF): a reference frame that observes the metric as flat and static. Then, the difference between any angular velocity Ω and the ZAMO, as seen from the LNRF, takes the form

$$U_{LNRF} = \frac{Af}{\rho} \left(1 - \frac{\Omega}{\omega} \right). \tag{15}$$

This result will be used later to investigate hypothetical streams of matter with angular velocity Ω.

3 The thin-shell formalism of General Relativity

The framework employed here is the thin-shell formalism, where the "shell" is what we refer to here as a surface. The formalism in itself is an exact approach to GR [17], but it makes assumptions and approximations easier.

A collection of two space-time manifolds $\mathcal{M}_+$ and $\mathcal{M}_-$ with their corresponding metrics, hypersurfaces $\Sigma_\pm$ and independent coordinate-systems can be glued to form a single hypersurface Σ by assuming that the metric is isometric [10], that is

$$g^+_{\mu\nu} = g^-_{\mu\nu}, \tag{16}$$

for all points in spacetime. The separating thin surface is characterized above- and below it by z and $-z$ respectively. This glued surface is illustrated in figure 7.

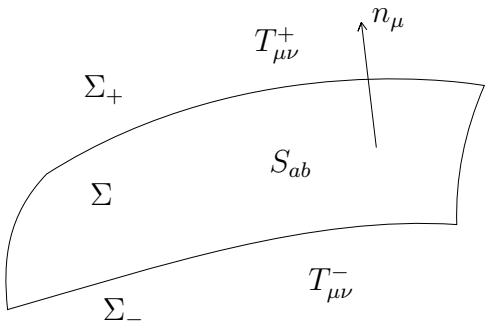

Figure 7: The surface Σ separates $\Sigma_\pm$ as a consequence of the glueing.

The surface in figure 7 is the cut-out region of the spacetime; we remove part of the spacetime defined by the metric and constrain the energy present to the surface defined as S_{ab} and assume that there is a vacuum everywhere else. We will refer to this as a gravitating disk - the surface will be composed of matter traveling alongside the surface. As the matter on the surface moves, the appearance of the surface will change. Still, the metric is time-independent, so the physical properties will not change unless the basis vectors (discussed below) are time-dependent.

Since $\Sigma_\pm$ is a submanifold to $\mathcal{M}_\pm$, we need to find the induced metric γ_{ab} defined on the hypersurface. We can rewrite a metric dependent on the coordinates x^μ, into another metric dependent on the coordinates in the hypersurface y^a by defining the vector basis $\frac{\partial x^\mu}{\partial y^a} = e_a{}^\mu$

$$ds^2 = g_{\mu\nu}\left(\frac{\partial x^\mu}{\partial y^a}dy^a\right)\left(\frac{\partial x^\nu}{\partial y^b}dy^b\right) \leftrightarrow \gamma_{ab} = e_a{}^\mu e_b{}^\nu g_{\mu\nu} \tag{17}$$

such that

$$\gamma^\pm_{ab} = e_a{}^\mu e_b{}^\nu g^\pm_{\mu\nu}, \tag{18}$$

where the Latin indices define the hypersurface's coordinates and where the greek indices describe the spacetime coordinates. The induced metric γ_{ab} is a two-tensor in three dimensions with a total of nine components and is used to raise and contract coordinates on the hypersurface y^a [17]. The vectors $e_a{}^\mu$ forms a vector-basis tangent to the surface, which defines the normal vector of the hypersurface n_μ

$$n_\mu e_a{}^\mu|_\pm = 0, \tag{19}$$

and where $n_\mu n^\mu|_+ = n_\mu n^\mu|_- = \varepsilon = \pm 1$. With these definitions, we can define the necessary components to calculate the energy-momentum tensor (SEMT) S_{ab} embedded in the surface. The expressions for its components will be derived in section 6-7.

The constant ε defines the spacelike (or timelike) nature of the hypersurface Σ:

$$n_\mu n^\mu = \varepsilon = \begin{cases} +1 & \text{Hypersurface is timelike} \\ -1 & \text{Hypersurface is spacelike} \end{cases}$$

Since the spacetime metric is isometric, it naturally follows that

$$\gamma^+_{ab} = \gamma^-_{ab}. \tag{20}$$

Although the metric is continuous, its derivatives are not [10]. Therefore, for hypersurfaces evaluated above and below, we have

$$\partial_\alpha g^{\mu\nu +} \neq \partial_\alpha g^{\mu\nu -}. \tag{21}$$

The conditions specified by Eq.(20-21) give rise to a non-vanishing extrinsic curvature K_{ab}: an important part of the thin-shell formalism, as it describes the three-dimensional curvature as seen in four-dimensional spacetime. In the following section, we shall derive it in full, along with the intrinsic covariant derivative, which describes how vector fields are differentiated along the surface.

3.1 Curvature on the surface

Before discussing the extrinsic curvature, it is a good idea first to discuss the intrinsic covariant derivative. As shall be seen later, the tensor-fields discussed in this thesis will be tangent to the surface i.e,

$$n_\mu A^{\mu\nu} = n_\mu e_a{}^\mu e_b{}^\nu A^{ab} = 0, \tag{22}$$

where we have used that any vector tangent to Σ can be decomposed using the basis vectors in the surface [17]

$$\begin{aligned} A^\mu &= e_a{}^\mu A^a \\ A_\mu &= e^a{}_\mu A_a = \gamma^{ab} g_{\mu\sigma} e_b{}^\sigma A_a \\ A^{P_1 P_2 \ldots P_i} &= e_{a_1}{}^{P_1} e_{a_2}{}^{P_2} \ldots e_{a_i}{}^{P_i} A^{a_1 a_2 \ldots a_i}. \end{aligned} \tag{23}$$

It is important to know how vectors fields are differentiated on the surface. Even though vectors are initially on the surface, they are not guaranteed to stay there as we transport them along a geodesic: the Christoffel symbols might contain terms orthogonal to the surface.

The surface is described by the induced metric γ_{ab} and is therefore equipped with a connection, defined through $\nabla_a \gamma_{bc} = 0$, different from that of the general spacetime coordinates, where the connection is defined through $\nabla_\mu g_{\alpha\beta} = 0$.

We define the intrinsic curvature as the projection of the covariant derivative in the spacetime connection onto the surface. This projection will be, in the following, denoted by a vertical line

$$A_{\mu;\nu} e_a{}^\mu e_b{}^\nu = A_{a|b}. \tag{24}$$

Expanding the expression in Eq.(24) is helpful because it allows us to see if a new set of Christoffel symbols can be easily defined. Using the product rule

$$A_{\mu;\nu} e_a{}^\mu e_b{}^\nu = \left(A_\mu e_a{}^\mu\right)_{;\nu} e_b{}^\nu - A_\mu e_a{}^\mu{}_{;\nu} e_b{}^\nu. \tag{25}$$

Eq.(25) can be simplified drastically. The first term boils down to the following result

$$\begin{aligned} \left(A_\mu e_a{}^\mu\right)_{;\nu} &= A_{\mu;\nu} e_a{}^\mu + A_\mu e_a{}^\mu{}_{;\nu} \\ &= e_a{}^\mu A_{\mu,\nu} - e_a{}^\mu \Gamma^\lambda{}_{\nu\mu} A_\lambda + A_\mu e_a{}^\mu{}_{,\nu} + A_\mu \Gamma^\mu{}_{\nu\lambda} e_a{}^\lambda \\ &= \left(A_\mu e_a{}^\mu\right)_{,\nu} = A_{a,\nu}. \end{aligned} \tag{26}$$

We can manipulate the second term in Eq.(25) to contain the contravariant form of A_a to relate the intrinsic covariant derivative to the spacetime equivalent properly. In other words, it would be desirable to read off the connection (Christoffel symbols) on the surface. This can be done by noting that,

$$\begin{aligned} A^\alpha e_{a\alpha;\beta} &= g^{\alpha\mu} A_\mu \left(g_{\alpha\nu} e_a{}^\nu\right)_{;\beta} \\ &= g^{\alpha\mu} A_\mu \left\{g_{\alpha\nu;\beta} e_a{}^\nu + g_{\alpha\nu} e_a{}^\nu{}_{;\beta}\right\} \\ &= \delta^\mu{}_\nu A_\mu e_a{}^\nu{}_{;\beta} = A_\alpha e_a{}^\alpha{}_{;\beta}. \end{aligned} \tag{27}$$

Using the results in Eq.(26-27) into Eq.(25), the intrinsic covariant derivative can be written in the form

$$A_{a|b} = A_{a,b} - \Gamma_{cab} A^c, \tag{28}$$

where the Christoffel symbols are defined by

$$\Gamma_{cab} = e_c{}^\gamma e_{a\gamma;\beta} e_b{}^\beta. \tag{29}$$

The intrinsic curvature derived here, is purely tangent to the surface, and is furthermore the tangential part of $A^\alpha{}_{;\beta} e_b{}^\beta$. The remaining question is whether or not a normal component to $A^\alpha{}_{;\beta} e_b{}^\beta$ exists. We start by decomposing the inverse metric $g^{\mu\nu}$ in terms of the normal- and basis vectors and the induced metric

$$g^{\mu\nu} = \varepsilon n^\mu n^\nu + \gamma^{ab} e_a{}^\mu e_b{}^\nu, \tag{30}$$

which satisfies

$$e^c{}_\mu e^d{}_\nu g^{\mu\nu} = \gamma^{cd} = \gamma^{ab} e_a{}^\mu e_b{}^\nu e^c{}_\mu e^d{}_\nu = \gamma^{ab} \delta_a{}^c \delta_b{}^d = \gamma^{cd}. \tag{31}$$

This is a useful decomposition, because $A^{\alpha}_{\ ;\beta} e_b^{\ \beta}$ can now be rewritten in terms of the mixed metric $g^{\mu}_{\ \nu} = \delta^{\mu}_{\ \nu}$

$$g^{\mu}_{\ \nu} A^{\nu}_{\ ;\beta} e_b^{\ \beta} = \lambda n_{\mu} A^{\mu}_{\ ;\beta} e_b^{\ \beta} n^{\alpha} + \gamma^{am} A_{\mu;\beta} e_m^{\ \mu} e_b^{\ \beta} e_a^{\ \alpha}. \tag{32}$$

Eq.(32) contains important information. It implies that $A^{\alpha}_{\ ;\beta} e_b^{\ \beta} n_{\alpha} \neq 0$, given by the first term in Eq.(32). Following the result derived in Eq.(28), we obtain

$$A^{\alpha}_{\ ;\beta} e_b^{\ \beta} = A^{a}_{\ |b} e_a^{\ \alpha} - \varepsilon A^{a} n^{\alpha} n_{\mu;\beta} e_a^{\ \mu} e_b^{\ \beta}. \tag{33}$$

We define the extrinsic curvature from the second term in Eq.(33), which is orthogonal to the surface

$$K_{ab} = n_{\alpha;\beta} e_a^{\ \alpha} e_b^{\ \beta}. \tag{34}$$

A good way to understand the physical property of extrinsic curvature is to imagine a cylindrical shape formed by a rolled-up piece of paper. The paper, in two dimensions, is flat (its intrinsic curvature is zero), but its cylindrical shape in three dimensions contains a non-vanishing curvature. This curvature is what we refer to as extrinsic curvature and is a way of measuring the curvature of lower-dimensional objects, as perceived in a higher dimension.

3.2 Nonvanishing extrinsic curvature

The extrinsic curvature evaluated in Σ_+ and Σ_- need not be equal, and their difference is nonvanishing. The reason is that the covariant derivative contains first-order derivatives of the metric in the Christoffel-symbols

$$\Gamma^{\nu}_{\ \mu\lambda} = \frac{1}{2} g^{\nu\beta} \left(\frac{\partial g_{\beta\mu}}{\partial x^{\lambda}} + \frac{\partial g_{\beta\lambda}}{\partial x^{\mu}} - \frac{\partial g_{\mu\lambda}}{\partial x^{\beta}} \right), \tag{35}$$

in which the derivatives are taken with respect to the spacetime coordinates. The discontinuities in the derivatives lead to a jump in extrinsic curvature, formulated as

$$K^{-}_{ab} - K^{+}_{ab} \neq 0. \tag{36}$$

All differences between the two submanifolds, such as Eq.(36), are formulated compactly as $[f] = f^{-} - f^{+}$. Since physical quantities have to be evaluated above- and below the surface, we will use a distributional approach that signifies these differences; the matter-energy density is restricted onto a thin shell on the cut-out region between Σ^{+} and Σ^{-}.

3.3 Surface energy-momentum tensor

The ingredients presented so far are required to formulate a theory of general relativity in 3 dimensions; in this case, they are time and two spatial coordinates. The extrinsic curvature allows us to find the SEMT $S_{\mu\nu}$ of a given surface bounded by $\Sigma_{\pm}$, as seen in

figure 7. First, let us formulate essential quantities used in Einsteins's field equations in a distributional way. Two hypersurfaces are present, as implied in the previous section. The parameter z signifies the distance along the normal direction from the surface, such that $z > b$ is above- and $z < -b$ is below the surface. Let us then define the metric tensor as

$$g_{\mu\nu} = \Theta(z-b)g^{+}_{\mu\nu} + \Theta(-z-b)g^{-}_{\mu\nu}, \tag{37}$$

where $\Theta(\pm z - b)$ is a modified Heaviside theta function (with an intermediate step where $\Theta(0) = 0$), indicating that only one part of the metric is present at any given point z in spacetime. Recall that we assume that the metric is isometric, i.e. it is continuous across the two hypersurfaces. However, its derivatives are not and are expressed explicitly as

$$g_{\mu\nu,\beta} = \Theta(z-b)g^{+}_{\mu\nu,\beta} + \Theta(-z-b)g^{-}_{\mu\nu,\beta} + \lambda\delta(z-b)[g_{\mu\nu}]n_{\beta}. \tag{38}$$

The last term comes from the chain-rule and that $\delta(x) = \delta(-x)$. This seems like a problem since $\delta(0)$ is undefined, but the bracketed quantity vanishes since the metric is isometric. Some problems appear to arise from the identification of Eq.(38) since $\delta(z-b)$ terms would appear in the Christoffel symbols. The presence of delta functions would imply infinities in the curvature, which is nonphysical. To see this, we express the Christoffel symbols like the metric in Eq.(37)

$$\Gamma^{\alpha}_{\ \beta\gamma} = \Theta(z-b)\Gamma^{\alpha+}_{\beta\gamma} + \Theta(-z-b)\Gamma^{\alpha-}_{\beta\gamma}. \tag{39}$$

The derivative will contain a non-vanishing $\delta(z-b)$ term because of the nature of Eq.(38)

$$\Gamma^{\alpha}_{\ \beta\gamma,\mu} = \Theta(z-b)\Gamma^{\alpha+}_{\beta\gamma,\mu} + \Theta(-z-b)\Gamma^{\alpha-}_{\beta\gamma,\mu} + \lambda\delta(z-b)[\Gamma^{\alpha}_{\ \beta\gamma}]n_{\mu}. \tag{40}$$

The Riemann tensor is expressed solely in terms of the Christoffel symbols (and thus the metric) as

$$R^{\rho}_{\ \sigma\mu\nu} = \Gamma^{\rho}_{\ \nu\sigma,\mu} - \Gamma^{\rho}_{\ \mu\sigma,\nu} + \Gamma^{\rho}_{\mu\lambda}\Gamma^{\lambda}_{\ \nu\sigma} - \Gamma^{\rho}_{\ \nu\lambda}\Gamma^{\lambda}_{\ \mu\sigma}. \tag{41}$$

Using the results of Eqs.(39-40) and substituting into Eq.(41), we find

$$R^{\alpha}_{\beta\gamma\delta} = \Theta(z-b)R^{\alpha+}_{\ \beta\gamma\delta} + \Theta(-z-b)R^{\alpha-}_{\ \beta\gamma\delta} + \delta(z-b)\lambda\left(\left[\Gamma^{\alpha}_{\ \beta\delta}\right]n_{\gamma} - \left[\Gamma^{\alpha}_{\beta\gamma}\right]n_{\delta}\right). \tag{42}$$

Once again, we find singularities at $z = b$, which we interpret as the surface where we glue the two hypersurfaces together. The task at hand is to find physical quantities on this surface, all embedded in the surface energy-momentum tensor S_{ab}. We start by looking at the $\delta(z-b)$ parts of the Christoffel symbols, Riemann tensor, and subsequently the Ricci scalar and using the conservation of energy to construct a surface equivalent of Einstein field equations. This is done by inserting the results of Eqs.(40-42) into the Einstein field equations and collecting all of the $\delta(z-b)$ terms. We can then find part of the full energy-momentum tensor $T_{\mu\nu}$ at the glued surface Σ.

The "surface" quantity in the Riemann tensor in Eq.(42) is dependent on the bracketed Christoffel symbols, and an explicit expression for it may be found with the identification that the discontinuity in $g_{\mu\nu,\beta}$ lies in the direction of the normal vector of the surface n_{μ}.

However, at first glance, it may seem that the quantity in the brackets of the surface term in Eq.(42) is not a tensor since there are Christoffel symbols, which, by themselves, do not transform like a tensor, as shown here for the transformation $x \to x'$:

$$\Gamma'^{\lambda}_{\ \mu\nu} = \frac{\partial x'^{\beta}}{\partial x^{\mu}} \frac{\partial x'^{\delta}}{\partial x^{\nu}} \frac{\partial x^{\lambda}}{\partial x'^{\gamma}} \Gamma^{\gamma}_{\ \beta\delta} + \frac{\partial x^{\lambda}}{\partial x'^{\sigma}} \frac{\partial^2 x'^{\sigma}}{\partial x^{\mu} \partial x^{\nu}}. \tag{43}$$

However, the difference $[\Gamma^{\mu}_{\ \alpha\beta}]$ transforms like a tensor, which is shown in the Appendix. Since the variation of the Christoffel symbols is a tensor, one can conclude that the bracketed term in Eq.(42) is a tensor, called $A^{\alpha}_{\ \beta\delta\gamma}$

$$A^{\alpha}_{\ \beta\delta\gamma} = \left[\Gamma^{\alpha}_{\ \beta\delta}\right] n_{\gamma} - \left[\Gamma^{\alpha}_{\ \beta\gamma}\right] n_{\delta}. \tag{44}$$

Since the discontinuity exists along the normal vector n_γ as mentioned earlier, the discontinuity in the derivative of the metric tensor can be expressed in terms of a new tensor. By multiplying the jump with $\varepsilon n_\gamma n^\gamma$,

$$\varepsilon [g_{\mu\nu,\gamma}] n_\gamma n^\gamma, \tag{45}$$

a new tensor can be defined by $\kappa_{\mu\nu} = \varepsilon [g_{\mu\nu,\gamma}] n^\gamma$. Hence we can express the discontinuity in terms of the new tensor

$$[g_{\mu\nu,\gamma}] = \kappa_{\mu\nu} n_\gamma. \tag{46}$$

With the definition in Eq.(46), we can find the expression for the surface-parts of the jump in Christoffel symbol, Riemann tensor $A^{\alpha}_{\ \beta\gamma\delta}$, Ricci tensor $A^{\mu}_{\ \alpha\mu\beta} = A_{\alpha\beta}$ and Ricci scalar $A^{\mu}_{\ \mu}$. They are given by (by noting that $\kappa = \kappa^{\mu}_{\ \mu}$)

$$\begin{aligned}
\left[\Gamma^{\alpha}_{\ \beta\gamma}\right] &= \frac{1}{2}\left(\kappa^{\alpha}_{\ \beta} n_\gamma + \kappa^{\alpha}_{\ \gamma} n_\beta - \kappa_{\beta\gamma} n^\alpha\right) \\
A^{\alpha}_{\ \beta\gamma\delta} &= \frac{\varepsilon}{2}\left(\kappa^{\alpha}_{\ \delta} n_\beta n_\gamma - \kappa^{\alpha}_{\ \gamma} n_\beta n_\delta - \kappa_{\beta\delta} n^\alpha n_\gamma + \kappa_{\beta\gamma} n^\alpha n_\delta\right) \\
A_{\alpha\beta} &= \frac{\varepsilon}{2}\left(\kappa_{\mu\alpha} n^\mu n_\beta + \kappa_{\mu\beta} n^\mu n_\alpha - \kappa n_\alpha n_\beta - \varepsilon \kappa_{\alpha\beta}\right) \\
A &= \varepsilon\left(\kappa_{\mu\nu} n^\mu n^\nu - \varepsilon\kappa\right).
\end{aligned} \tag{47}$$

Now all of the relevant surface terms have been defined to successfully express the surface energy-momentum tensor $S_{\mu\nu}$. Finally, substituting in the expressions for the Ricci tensor and its corresponding scalar and collecting the $\delta(z-b)$ terms, one can make the identification for the full energy-momentum tensor that it is composed of three parts: one in either hypersurface and one on the surface itself

$$T_{\mu\nu} = \Theta(z-b) T^{+}_{\mu\nu} + \Theta(-z-b) T^{-}_{\mu\nu} + \delta(z-b) S_{\mu\nu}. \tag{48}$$

Using the expressions found in Eq.(47), $S_{\mu\nu}$ can be readily defined

$$\begin{aligned}
S_{\mu\nu} &= A_{\mu\nu} - \frac{1}{2} A g_{\mu\nu} \\
&= \frac{1}{16\pi\varepsilon}\left\{\kappa_{\mu\alpha} n^\mu n_\beta + \kappa_{\mu\beta} n^\mu n_\alpha - \kappa n_\alpha n_\beta - \varepsilon\kappa_{\alpha\beta} - \left(\kappa_{\mu\nu} n^\mu n^\nu - \varepsilon\kappa\right) g_{\alpha\beta}\right\}.
\end{aligned} \tag{49}$$

One can change the coordinate basis of $S_{\mu\nu}$ to the surface coordinates a and b by a normal coordinate transformation

$$S_{ab} = S_{\mu\nu}\frac{\partial x^\mu}{\partial x^a}\frac{\partial x^\nu}{\partial x^b} = S_{\mu\nu}e_a{}^\mu e_b{}^\nu, \tag{50}$$

where $e_a{}^\mu$ compose the vector basis discussed earlier. Note that many terms in Eq.(49) are normal to the surface, so

$$\begin{aligned} 16\pi S_{ab} &= -\kappa_{\mu\nu}e_a{}^\mu e_b{}^\nu - \varepsilon\left(\kappa_{\mu\nu}n^\mu n^\nu - \varepsilon\kappa\right)\gamma_{ab} \\ &= -\kappa_{\alpha\beta}e_a{}^\alpha e_b{}^\beta + \gamma_{ab}\gamma^{cd}\left(\kappa_{\alpha\beta}e_c{}^\alpha e_d{}^\beta\right). \end{aligned} \tag{51}$$

The question now is what the three-tensor $\kappa_{\alpha\beta}e_a{}^\alpha e_b{}^\beta$ actually is. We know that z is continuous as we cross the surface, and so $[n_\alpha] = 0$. Secondly, the coordinates are the same above- and below the surface, yielding $[e_a{}^\alpha] = 0$. We can therefore take a look at the jump in the covariant derivative of the normal vector in the surface

$$[n_{\alpha;\beta}] = \left[e^a{}_\beta\partial_a n_\alpha - \Gamma^\lambda{}_{\alpha\beta}n_\lambda\right] = -\left[\Gamma^\lambda{}_{\alpha\beta}\right]n_\mu, \tag{52}$$

where the first term vanish, since n_α is normal to the surface. Substituting the result for the jump in the Christoffel symbols in Eq.(47) we obtain

$$[n_{\alpha;\beta}] = \frac{1}{2}\left(\varepsilon\kappa_{\alpha\beta} - \kappa_{\gamma\alpha}n_\beta n^\gamma - \kappa_{\gamma\beta}n_\alpha n^\gamma\right), \tag{53}$$

yielding

$$[K_{ab}] = \frac{\varepsilon}{2}\kappa_{\alpha\beta}e_a{}^\alpha e_b{}^\beta. \tag{54}$$

This allows us to rewrite Eq.(51) in terms of the jump in extrinsic curvature

$$S_{ab} = -\frac{\varepsilon}{8\pi}\left([K_{ab}] - \gamma_{ab}[K^c{}_c]\right). \tag{55}$$

Eq.(55) describes the physical properties confined to the defined surface. It serves as a variant to Einstein's field equations and helps in physical configurations concerning boundary problems in General Relativity, such as matching interior and exterior solutions of two different spacetimes. A famous example is that of Oppenheimer and Snyder, where they discussed gravitational collapse for stationary, spherical massive bodies by matching the Schwarzschild- and FLRW metric at the surface [3], which can now be done easily by matching the extrinsic curvature instead.

In essence, the thin-shell formalism is helpful because it effectively removes dimensions (depending on your surface basis-vectors) by restricting the part of spacetime we consider in our calculations. The simplicity that comes with Eq.(55) lies in that it reduces the size of the stress-energy tensor, making eigenvalue-problems easier compared to the original size of $T^{\mu\nu}$ that is 4×4. We see that the discontinuity of the metric tensor causes the curvature to be discontinuous. This discontinuity causes a nonzero difference between its value above- and below the surface, and it is this jump that causes the surface to gravitate.

4 Energy conditions

A useful technique to examine the matter-energy content present in any system is to decompose it into a set of vectors, for example

$$T^{\mu\nu} = \sigma V^{\mu} V^{\nu} + P_1 W_1^{\mu} W_1^{\nu} + P_2 W_2^{\mu} W_2^{\nu} + P_3 W_3^{\mu} W_3^{\nu}, \tag{56}$$

where V and W are vectors that contain the information about how the matter that makes up $T^{\mu\nu}$ moves. A successful vector decomposition can unfold the trajectories of matter that build $T^{\mu\nu}$ if the matter distribution is physically possible, i.e., not violating any energy conditions. As an example, in section 6, it will be shown that one possible matter-distribution is that of two counter-rotating streams of matter confined to a disk. It will be used to construct a static, rotating source to the Kerr metric. The numerical values of σ and P_i denote the density and pressures present in the system. To ensure that the vectors obtained through the decomposition (along with the density and pressures) are physical, they collectively need to satisfy certain energy conditions.

Much like we discard the negative energies of particles in classical and quantum mechanical theories, general relativistic criteria have been developed to ensure the physicality of the vectors that decompose the stress-energy tensor. As a specific example, the vectors should not have negative energy densities. In total, there are four energy conditions: *weak*, *null*, *strong*, and *dominant*. In this thesis, we will consider matter only, and since the null energy condition concerns massless particles, we will not consider it here.

To investigate the energy conditions in more detail, we will consider an arbitrary time-like vector U^{μ}, which will be assumed to be normalized accordingly

$$U^{\mu} U_{\mu} = -1. \tag{57}$$

4.1 Weak energy condition (WEC)

The weak energy condition states that, for any time-like vector $U^{\mu} = d(1, a, b, c)$, with $d = (1 - a^2 - b^2 - c^2)^{1/2}$ we have

$$T^{\mu\nu} U_{\mu} U_{\nu} \geq 0. \tag{58}$$

Eq.(58) can be expanded to give

$$\sigma + a^2 P_1 + b^2 P_2 + c^2 P_3 \geq 0, \tag{59}$$

where the normalization condition determines the coefficients. The density cannot be negative, but the pressure can be positive or negative (representing tension.) Therefore the weak energy condition requires that the density is larger than or equal to zero: $\sigma \geq 0$. Since the pressures can be negative, another equality is required: the coefficients in Eq.(59) are arbitrary since the WEC should hold for any basis; if $b = c = 0$, together with the normalization condition that $a < 1$, then $\sigma + P_i > 0$. Put in words, WEC states that, for any observer defined on an arbitrary basis, the matter-energy content must be non-negative.

4.2 The strong energy condition (SEC)

The strong energy condition is a statement of the curvature of the spacetime itself. The statement, using the same basis as in the previous section, reads

$$\left(T_{\mu\nu} - \frac{1}{2}T g_{\mu\nu}\right) U^\mu U^\nu = 8\pi R_{\mu\nu} U^\mu U^\nu \geq 0, \tag{60}$$

where $R_{\mu\nu}$ is the Ricci tensor. It says that, for any observer, the tidal tensor is always positive. The surface equivalent of the strong energy condition refers to the extrinsic curvature, as can be seen through their connection in Eq.(55).

The statement should, as for the WEC, hold for any normalized, future-directed timelike vector. Hence

$$d^2(\sigma + a^2 P_1 + b^2 P_2 + c^2 P_3) \geq \frac{1}{2}(\sigma - \sum_i P_i), \tag{61}$$

for arbitrary values of a, b, c and d specified through the choice of basis and normalization. This statement does not explicitly say anything about the system's density but rather the combination of the density and pressures. This time, the sum of the pressures and density is greater than or equal to zero

$$\sigma + \sum_i P_i \geq 0. \tag{62}$$

We also find that the sum of any pressure component and the density may be zero

$$\sigma + P_i \geq 0. \tag{63}$$

4.3 Dominant energy condition (DEC)

The final energy condition considered in this thesis is the dominant energy condition (DEC). The DEC states that for an arbitrary vector field U^μ that is both timelike and future-directed, then

$$-T^\mu_{\ \nu} U^\nu \tag{64}$$

is also a timelike/null, future-directed vector field. Once again, by expanding

$$\sigma^2 - a^2 P_1^2 - b^2 P_2^2 - c^2 P_3^2 \geq 0. \tag{65}$$

Since this condition should hold for any configuration of a, b and c, and requiring that the vector be timelike and future-directed, the statement requires the following inequalities:

$$\sigma \geq 0, \quad \sigma \geq |P_i|. \tag{66}$$

This is a statement about the cosmic speed limit; matter, nor energy, can flow faster than the speed of light for any observer. No matter what vector basis is chosen, the matter-energy content will always follow a time-like vector.

5 Properties of gravitating disks

As briefly mentioned in the introduction, a gravitating disk is a surface composed of matter which flows around in it. Here, we construct such a disk by defining a set of surface basis-vectors and projecting the Kerr metric onto that surface. To discuss the properties of gravitating disks in the general case, one has to start with defining the mentioned vector basis. Such a basis can be chosen intuitively for specific purposes. In this thesis, we choose a time-dependent vector basis to investigate how the surface collapses with time, which is an extension of [8] and [9]. We have three basis-vectors inside the surface, together with a normal vector orthogonal to them such that

$$e_a{}^{\mu} n_{\mu} = 0. \tag{67}$$

For a collapsing surface with coordinates $y^a = (t, \phi, s)$, embedded in a spacetime with coordinates $x^{\mu} = (t, \phi, \rho, z)$, we impose the dependence $\rho \to \rho(t, s)$ and $z \to z(t, s)$. We then obtain

$$e_a{}^{\mu} = \frac{\partial x^{\mu}}{\partial y^a} = \begin{pmatrix} 1 & 0 & \dot{\rho} & \dot{z} \\ 0 & 1 & 0 & 0 \\ 0 & 0 & \rho' & z' \end{pmatrix}. \tag{68}$$

Where $\dot{f}$ denotes the time-derivative of f and f' denotes the s-derivative respectively. The form of the basis-vectors expresses that they change with time, such that the ρ- and z-components no longer remain constant, as desired. Moreover, here we assume that the surface shape is not completely "flat" in relation to ρ, meaning that the distance from the center in the surface s changes with the spacetime distance ρ up to some function. Furthermore, the absence of a basis-vector in the z-direction implies that all further tensors given in the surface coordinates will be 3×3 in nature. Let us now define a normal vector of the form:

$$n_{\mu} = (a, b, c, d), \tag{69}$$

and try to find its components. Eq.(67) then provides the following system of equations:

$$\begin{aligned} 0 &= a + \dot{\rho} c + \dot{z} d \\ 0 &= b \\ 0 &= \rho' c + z' d. \end{aligned} \tag{70}$$

The normal vector then becomes

$$n_{\mu} = \lambda \left(\rho' \dot{z} - \dot{\rho} z', 0, -z', \rho' \right), \tag{71}$$

where λ is a function of s and t. The next step is to find the explicit form of λ to make it unit-normal, and for that, a metric is required. The spacetime of interest is that of a rotating, axially symmetric metric, from Eq.(4). This sets the requirement on λ

$$\lambda^2 = \pm \left\{ \frac{A^2 f^2 - \rho^2}{\rho^2 f} [\dot{\rho} z' - \rho' \dot{z}] + \frac{f}{h} [z'^2 + \rho'^2] \right\}, \tag{72}$$

where the $\pm$ denotes if the vector is time-like or space-like, respectively.

With the normal vector in hand, we can calculate the extrinsic curvature of the surface defined in Eq.(34). This yields the following results (with indices in brackets indicating surface coordinates):

$$
\begin{aligned}
\frac{K_{(t)(t)}}{\lambda\alpha} &= \frac{\ddot{\rho}z' - \rho'\ddot{z}}{\alpha} - 2h(\dot{\rho}z' - \rho'\dot{z})(\dot{\rho}R_\rho + \dot{z}R_z) \\
&\quad - \rho^2\left[(\dot{\rho}^2 - \dot{z}^2)(z'H_\rho - \rho' H_z) - 2\dot{\rho}\dot{z}(\rho' H_\rho - z' H_z)\right] \\
&\quad - \rho^2 f^2\left(\rho'\frac{\partial f}{\partial z} - z'\frac{\partial f}{\partial \rho}\right) \\
\frac{K_{(t)(\phi)}}{\lambda} &= -\frac{1}{2}\left[\frac{(\dot{\rho}z' - \rho'\dot{z})}{f\rho^2}(\dot{\rho}K_\rho + \dot{z}K_z - 2fA\rho) + \frac{f}{h}(\rho' L_z - z' L_\rho)\right] \\
\frac{K_{(t)(s)}}{\lambda\alpha} &= \frac{z'(\dot{\rho})' - \rho'(\dot{z})'}{\alpha} - (\dot{\rho}z' - \rho'\dot{z})(\rho' R_\rho + z' R_z) - \rho^2\left[H_z(z'^2\dot{\rho} + \rho'^2\dot{z}) - H_\rho(z'^2\dot{z} + \rho'^2\dot{z})\right] \\
\frac{K_{(\phi)(\phi)}}{\lambda\alpha} &= -\rho^2\left[z'(E_\rho - 2\rho f) + \rho' E_z\right] \\
\frac{K_{(\phi)(s)}}{\lambda\alpha} &= -h(\dot{\rho}z' - \rho'\dot{z})(z' K_z + \rho'\left[K_\rho - 2fA\rho\right]) \\
\frac{K_{(s)(s)}}{\lambda\alpha} &= \rho^2\left[\frac{z'\rho'' - \rho' z''}{\alpha} - (z'^2 + \rho'^2)(\rho' H_z - z' H_\rho)\right],
\end{aligned}
$$

where the functions $H_x, R_x, K_x, L_x, E_x, F_x$ and α are given by:

$$
\begin{aligned}
H_x &= h\frac{\partial f}{\partial x} - f\frac{\partial h}{\partial x} \\
R_x &= f^3 A\frac{\partial A}{\partial x} + \rho^2\frac{\partial f}{\partial x} \\
K_x &= f^3 A^3\frac{\partial A}{\partial x} + f\rho^2\frac{\partial A}{\partial x} + 2A\rho^2\frac{\partial f}{\partial x} \\
L_x &= A\frac{\partial f}{\partial x} + f\frac{\partial A}{\partial x} \\
E_x &= 2f^3 A\frac{\partial A}{\partial x} + A^2 f^2\frac{\partial f}{\partial x} + \rho^2\frac{\partial A}{\partial x} \\
F_x &= \left(\frac{\partial z}{\partial x}\right)^2 + \left(\frac{\partial \rho}{\partial x}\right)^2 \\
\alpha &= 2f\rho^2 h.
\end{aligned}
$$

An important observation is that all of the components in the extrinsic curvature are odd in z, meaning that the jump takes on the form

$$
[K_{ab}] = -2K^+_{ab}. \tag{73}
$$

In this thesis, we choose a timelike normalization of the normal vector such that $\varepsilon = 1$ (see section 3). Using Eq.(73), the SEMT can be described entirely through the extrinsic

curvature evaluated above the surface

$$S_{ab} = \frac{1}{4\pi}\left(\gamma_{ab}K^{+} - K^{+}_{ab}\right), \tag{74}$$

where the induced metric is given by

$$\gamma_{ab} = \frac{1}{f}\begin{pmatrix} -f^2 + h\dot{\rho}^2 + h\dot{z}^2 & -f^2A & h\left(\dot{z}z' + \dot{\rho}\rho'\right) \\ -f^2A & -f^2A^2 + \rho^2 & 0 \\ h\left(\dot{\rho}\rho' + \dot{z}z'\right) & 0 & h\left((z')^2 + (\rho')^2\right). \end{pmatrix} \tag{75}$$

The resulting expressions are very long, and so only limiting cases will be presented in this thesis.

6 Limiting cases

For demonstration purposes, we will consider the case for a static, infinitely wide disk due to the removed part of the spacetime, i.e., our glued surface. We will follow the results of [8, 9] in sections 6-6.2 to show that a possible source of the Kerr metric can be obtained through diagonalization of the SEMT and that geodesic streams give rise to negative energy densities. In this case, the basis vectors are invariant under time translations, and so $\dot{\rho} = \dot{z} = 0$. Furthermore, since the disk is infinitely long with a constant z, we find that $z' = 0$, such that the width of the disk remains unchanged with changing distance from the center inside the surface. Finally, we make the additional assumption that ρ changes linearly with the distance inside the surface, s, and so $\rho' = 1$. This yields the following basis vectors and the corresponding normal vector

$$e_a{}^{\mu} = \begin{pmatrix} 1 & 0 & 0 & 0 \\ 0 & 1 & 0 & 0 \\ 0 & 0 & 1 & 0 \end{pmatrix}, \quad n_{\mu} = \lambda\left(0, 0, 0, 1\right), \tag{76}$$

where λ acquires the form from Eq.(72)

$$\lambda = \pm\left(\frac{h}{f}\right)^{1/2}. \tag{77}$$

The non-zero components of the extrinsic curvature are given by:

$$K_{(t)(t)} = -\frac{\lambda}{2h}\frac{\partial f}{\partial z}f \qquad K_{(t)(\phi)} = -\frac{\lambda}{2h}fL_z \tag{78}$$

$$K_{(\phi)(\phi)} = -\frac{\lambda}{2fh}E_z \qquad K_{(s)(s)} = -\frac{\lambda}{2fh}H_z. \tag{79}$$

By using the basis-vectors in Eq.(76) together with Eq.(18), we find the induced metric γ_{ab} and its inverse

$$\gamma_{ab} = e_a{}^{\mu} e_b{}^{\nu} g_{\mu\nu} = \begin{pmatrix} -f & -fA & 0 \\ -fA & \frac{\rho^2 - f^2A^2}{f} & 0 \\ 0 & 0 & \frac{h}{f} \end{pmatrix} \quad \gamma^{ab} = \begin{pmatrix} \frac{f^2A^2 - \rho^2}{\rho^2 f} & -\frac{Af}{\rho^2} & 0 \\ -\frac{Af}{\rho^2} & \frac{f}{\rho^2} & 0 \\ 0 & 0 & \frac{f}{h} \end{pmatrix}, \tag{80}$$

yielding the trace of the extrinsic curvature

$$K = K^a{}_a = \gamma^{ab} K_{ab} = -\frac{\lambda}{2h^2} H_z. \tag{81}$$

If K is negative, a family of geodesics converges with proper time, contrary to when it is positive, where the congruence is diverging [18]. Moreover, the trace of the extrinsic curvature is odd in z, implying that a family of geodesics intersecting the disk's surface will converge towards the center when approaching from above and diverge from it when approaching from below the disk. Consequently, when evaluated on the surface, the extrinsic curvature is on average equal to zero. We show the trace of the extrinsic curvature in figure 8, in terms of the circumferential radius $R = \sqrt{g_{\phi\phi}}$ and for constant values of b such that the central density of the disks is positive, i.e., $\sqrt{M^2 - a^2} < b < M^2/2a$, which will be explained in section 6.1.

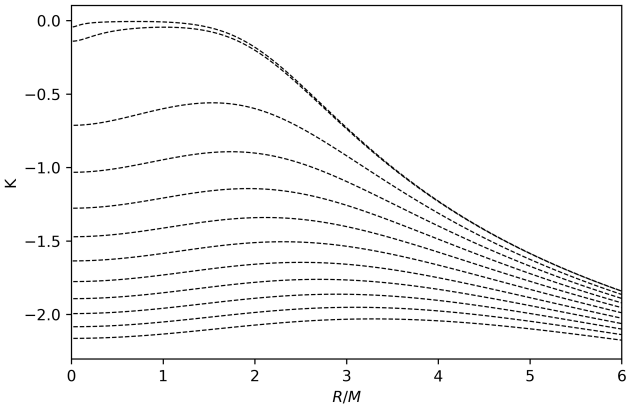

Figure 8: The trace of the extrinsic curvature is negative for $R/M \geq 0$, suggesting that geodesics converges towards the center at constant $b/M = [0.6013, 0.613, 0.87, 1.11, 1.34, 1.56, 1.78, 2.00, 2.21, 2.42, 2.63, 2.84]$

Since all terms are odd in z, we may use the result derived in Eq.(74). The non-zero

elements of the SEMT then become

$$\begin{aligned} S_{(t)(t)} &= -\frac{f\lambda}{8\pi h^2}\left[f\frac{\partial h}{\partial z} - 2h\frac{\partial f}{\partial z}\right], \\ S_{(t)(\phi)} &= \frac{\lambda f}{8\pi h^2}\left[h\left(f\frac{\partial A}{\partial z} + 2A\frac{\partial f}{\partial z}\right) - Af\frac{\partial h}{\partial z}\right], \\ S_{(\phi)(\phi)} &= \frac{\lambda}{8\pi h^2}\left[2Af^2h\frac{\partial A}{\partial z} + 2A^2fh\frac{\partial f}{\partial z} + \frac{\partial h}{\partial z}\left(\rho^2 - A^2f^2\right)\right]. \end{aligned} \tag{82}$$

The SEMT can be decomposed as a sum of outer products between vectors

$$S_{ab} = \sigma V_a V_b + P W_a W_b, \tag{83}$$

where the vectors V, W express the structure of the matter (an ideal gas with surface density σ and surface pressure P) that builds up the SEMT through diagonalization with the conditions that $V^2 = -1$, $W^2 = 1$ and $V.W = 0$. We will refer to them as being $\phi-$isotropic, because they are independent on ϕ.

Another simple model concerns that of two counter-rotating streams of matter that follow geodesics, where we choose the vectors to have the form

$$U^\mu_\pm = N_\pm\left[1, \Omega_\pm, 0, 0\right], \tag{84}$$

where $\Omega_\pm$ are the angular velocities of the rotating streams.

We will refer to such streams in Eq.(83) and (84) as *configurations* of matter. The components can be derived in various cases, and in this section, the $\phi-$isotropic case and the geodesic case will be discussed.

6.1 ϕ-isotropic observer of the stationary SEMT

In the so-called $\phi-$isotropic frame, the SEMT in Eq.(82) obtains a diagonal form

$$\begin{aligned} V_\mu V_\nu S^{\mu\nu} &= \sigma, \\ W_\mu W_\nu S^{\mu\nu} &= P, \\ V_\mu W_\mu S^{\mu\nu} &= 0, \end{aligned} \tag{85}$$

where the vectors, along with the SEMT, are expressed in terms of the spacetime coordinates. The system given in Eq.(83) posits that V, W are *eigenvectors* of the SEMT and σ, P are the *eigenvalues* respectively. This enforces the criteria that $V^\mu W_\mu = 0$, and the vectors are chosen such that $V^\mu V_\mu = -1$ together with $W^\mu W_\mu = 1$. If the vectors have the form

$$\begin{aligned} V^\mu &= N(1, \Omega, 0, 0) \\ W^\nu &= J(\beta, 1, 0, 0), \end{aligned} \tag{86}$$

then we obtain the following solutions to Eq.(85):

$$\begin{aligned} N &= \left[\frac{f}{f^2-\Omega^2\rho^2-\Omega f^2 A(\Omega A+2)}\right]^{1/2}, \\ J &= \frac{f(A\Omega+1)}{\rho}N, \\ \beta &= \frac{\Omega\rho^2-f^2A(A\Omega+1)}{f^2(A\Omega+1)}, \\ \Omega &= \frac{S^{\phi\phi}-S^{tt}-\sqrt{(S^{\phi\phi}-S^{tt})^2+4S^{t\phi}S^{t\phi}}}{2S^{t\phi}}. \end{aligned} \tag{87}$$

The diagonalization of the SEMT in Eq.(85) also determines the eigenvalues

$$\sigma = \frac{S^{tt}-\beta^2 S^{\phi\phi}}{N^2(1-\beta^2\Omega^2)}, \quad P = \frac{S^{tt}-\Omega^2 S^{tt}}{J^2(1-\beta^2\Omega^2)}. \tag{88}$$

As demonstrated, the parameters have been obtained solely through orthogonality, normalization, and diagonalization, not by using the geodesic equations demonstrated in the next section. This implies that the results in Eqs.(87-88) may not follow geodesics, and might just be a non-physical distribution of matter that acts as a source to the Kerr metric.

Some interesting physical properties can nevertheless be deduced. For example, the horizon density (σ evaluated at $R/M=0$) obtains the form

$$\sigma(R/M=0) = \frac{1}{2\pi}\frac{M\left((M^2+b^2)^2-a^2\right)}{\left((M^2+b^2)^2-a^2\right)^{3/2}\sqrt{a^2+b^2-M^2}}. \tag{89}$$

The positivity of the central density sets a lower bound on b concerning the mass of the source and its angular momentum, $b > \sqrt{M^2-a^2}$. By using the results found in section 2, an upper- and lower bound is found for generating ergoregions, confining b accordingly

$$\sqrt{1-\frac{a^2}{M^2}} < \frac{b}{M} < \frac{M}{2a}. \tag{90}$$

In the following, the physical properties of the disks will concern a value of angular momentum-to-mass quotient as $a/M = 0.8$. Hence $0.6 < b/M < 0.625$ to construct disks with ergoregions. For very relativistic disks (with low values of b), the central density follows up to first-order near the lower bound of $b \approx \sqrt{M^2-a^2}$ at $a = 0.8M$

$$\sigma(0) \approx \frac{4.9\cdot 10^{-2}}{\sqrt{bM-0.6M^2}}. \tag{91}$$

Following the discussion in section 2, the velocity V (the $\phi-$isotropic frame) can be observed through the LNRF frame. Thus, we can express the velocity as

$$V = -\frac{f}{\rho}\left(\Omega - \frac{A}{\frac{\rho^2}{f^2}-A^2}\right), \tag{92}$$

in which Ω is given by Eq.(87). Furthermore, two rotating streams of matter around a point coinciding with the origin can rotate with the same velocity relative to the new $\phi-$isotropic frame of reference. The velocity, denoted herein by U, is related directly to the eigenvalues of the SEMT

$$U = \sqrt{\frac{P}{\sigma}}. \tag{93}$$

The analytical expressions for the velocities are long and so only a graphical representation will be provided. They are shown in figure 9, in terms of a circumferential radius $R = \sqrt{g_{\phi\phi}}$.

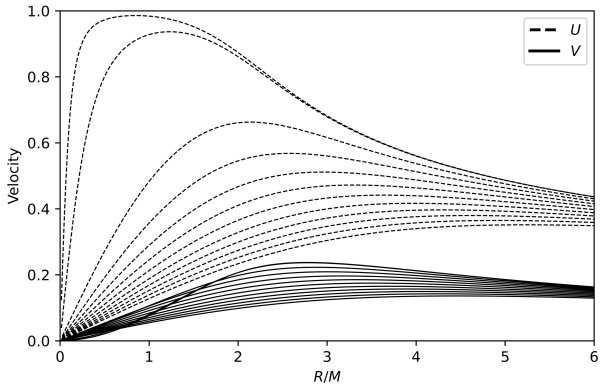

Figure 9: The dashed lines are the velocities of the streams U, as seen by the $\phi-$isotropic basis. The solid lines are the velocities of the $\phi-$isotropic basis relative to the LNRF frame. A total of twelve curves are presented, each corresponding to (from top to bottom in each case) a different value of $b/M = [0.6013, 0.613, 0.87, 1.11, 1.34, 1.56, 1.78, 2.00, 2.21, 2.42, 2.63, 2.84]$.

The two upper velocities of the disks, measured in the $\phi-$isotropic basis, approach the speed of light near $R/M \approx 1$ but decrease to zero at $R/M = 0$. There are no singularities at play, neither for the stream's velocities nor the $\phi-$isotropic basis observed by the LNRF. Furthermore, only the top two curves produce an ergoregion in accordance with the lower- and upper bound of b to produce such regions. It shows that the disks become increasingly relativistic for smaller values of b, which, concerning the nature of the central density, is sensible; a smaller b comes with a higher density.

As observed from the LNRF frame, the $\phi-$isotropic frame rotates the fastest at $R/M \approx 2.6$ and is relatively slow near the center, including the ergoregion-producing disks. The densities of these disks are all finite at $R = 0$, except those that produce the ergoregions, as shown in figure 10.

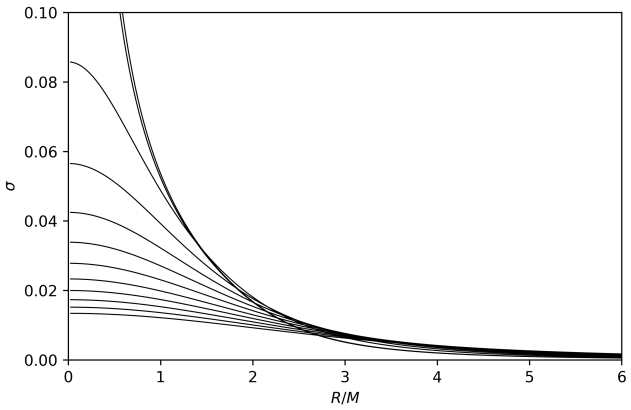

Figure 10: The density σ of the ergoregion-producing disks has an undefined limit at a zero circumferential radius. On the other hand, the disks that do not produce an ergoregion have a finite mass density at the $R/M = 0$. Further, the density of the disks falls rapidly and starts to converge at $R/M \approx 3$.

From figure 10 we see that the most relativistic disk densities (disks that produce the highest angular velocities) decrease faster than in the nonrelativistic case, suggesting that the disk's mass gets increasingly confined to the center.

The density in figure 10 reveals that it is positive everywhere for all configurations. Therefore only the secondary inequalities presented in section 4 will be shown in figure 11 a) and b).

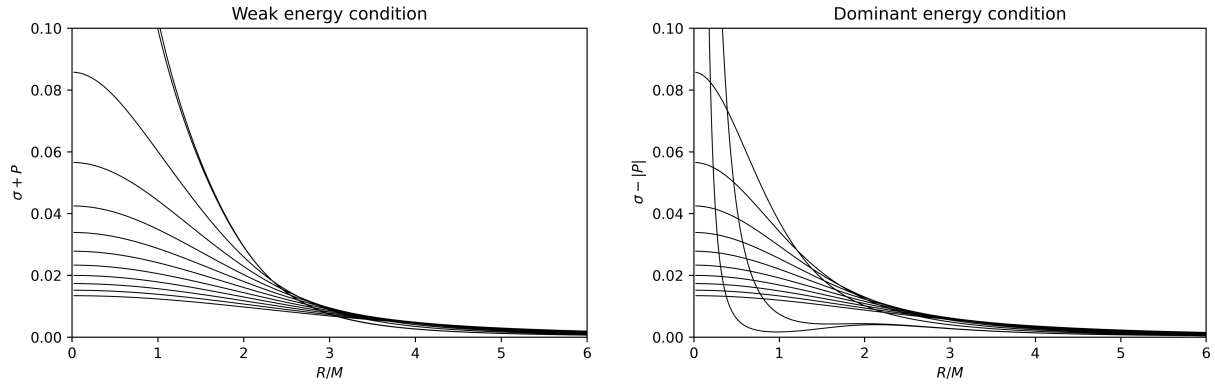

(a) The sum of the density and pressure of the configuration.

(b) The difference between the density and absolute value of the pressure.

Figure 11: a): As required for the weak energy condition (WEC), the sum of the eigenvalues (or densities and pressures) should be larger than or equal to zero. The WEC is satisfied for all configurations and has an undefined limit for the ergoregion-producing disks (the two upper curves). In b), it is shown that the dominant energy condition is satisfied for all configurations.

Both the WEC and DEC are satisfied for the twelve physical configurations considered. Interestingly, figure 11 (b) can be interpreted as the proper rest mass as observed from the $\phi-$isotropic frame [8], revealing that the mass attains its minimum when the $\phi-$isotropic frame approaches the speed of light $U \approx 1$ in the ergoregion-producing disks.

6.2 Counter-rotating geodesic streams (CRGS)

As discussed in section 6, a two-by-two SEMT can be built up with two vectors U_+ and U_- according to Eq.(56) with the form in Eq.(84). Contrary to the previous section, the parameters will have to satisfy the geodesic equation in the hope of finding a model that is better physically. From the basis-vectors in Eq.(76), the spacetime form of any surface vector takes the form

$$U^\mu = e_a{}^\mu U^a = \delta_a{}^\mu U^a. \tag{94}$$

Now an important observation has to be made. If the spacetime is viewed as a cross-section in the (z, x)-plane, then a cut-out region is present between $-b < z < b$, as illustrated in figure 2, but will be shown here again for visibility in figure 12.

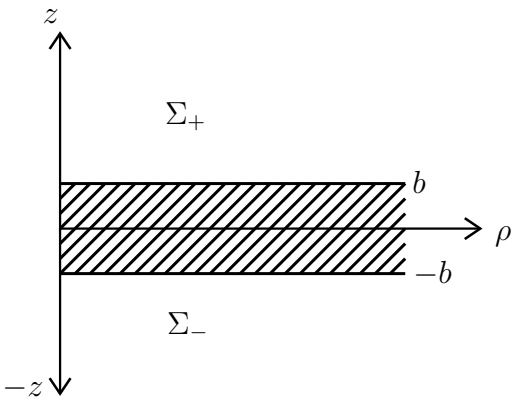

Figure 12: The region in $-b < z < b$ is a cutoff in the spacetime. A particle on the surface has to obey the geodesic equation both at b and $-b$ simultaneously.

All four of the geodesic equations are expressed as

$$U^\alpha U^\mu{}_{,\alpha} + \Gamma^\mu{}_{\alpha\beta} U^\alpha U^\beta = 0. \tag{95}$$

Some of the geodesic equations are automatically satisfied. To see this, symmetry arguments has to be made. When the surface is viewed from the spacetime coordinates, and we want to evaluate a function $f(x)$ on the surface Σ, we will use the concept of *arithmetic mean*, introduced by [10]

$$\tilde{f} = f^+ \Theta(z-b) + f^- \Theta(-z-b). \tag{96}$$

Where the Θ functions are step functions with an additional intermediate step

$$\Theta(X) = \begin{cases} 1, & X > 0 \\ \frac{1}{2}, & X = 0 \\ 0, & X > 0 \end{cases}. \tag{97}$$

The intermediate step functions allow for evaluation of functions at the surface, such that it is the average of the function below- and above it, respectively [10]. The metric is the same above- and below the surface so we find $\tilde{g}_{\mu\nu} = g_{\mu\nu}$. However, the metric's derivatives are not, so the Christoffel symbols need to be averaged when evaluated over the surface. Therefore, all of the terms in the geodesic equations that are odd in z will cancel at the surface. The fourth geodesic equation is entirely odd and is therefore not considered when calculating the trajectories of particles initially at the surface, as the average amounts to zero.

Consequently, it is found that the only surviving equation needed to be solved is the ρ-component of the geodesic equation (with the t, ϕ and z equations being solved automatically by $0 = 0$)

$$e^a{}_\mu U^\alpha U^\mu{}_{;\alpha} = \frac{\partial f}{\partial \rho}\left[(A\Omega_\pm + 1)^2 f^2 + \rho^2 \Omega_\pm^2\right] - 2f\Omega_\pm \left[\rho\Omega_\pm - f^2 \frac{\partial A}{\partial \rho}(A\Omega_\pm + 1)\right] = 0. \tag{98}$$

The derivation of this equation is shown in the appendix. There are two solutions to this equation, representing opposite directional motion. They are:

$$\Omega_{\pm} = -\frac{f\left(A_{,\rho}f^2 + Aff_{,\rho} \pm \sqrt{f^4A_{,\rho}^2 - \rho^2 f_{,\rho}^2 + 2f\rho f_{,\rho}}\right)}{2f^3AA_{,\rho} + A^2f^2f_{,\rho} + \rho^2 f_{,\rho} - 2\rho f}. \tag{99}$$

The normalization condition

$$N_{\pm}^2 = \frac{-1}{g_{\phi\phi}\Omega_{\pm}^2 + 2g_{t\phi}\Omega_{\pm} + g_{tt}}, \tag{100}$$

fully determines the components in the tensor fields and ensures that they are normalized to -1. Now the vector decomposition of the SEMT can be used to find the density and pressure of the configuration

$$\mu_{\pm} = \pm\left(g_{\phi\phi}\Omega_{\pm}^2 + 2g_{t\phi}\Omega_{\pm} + g_{tt}\right)\frac{\Omega_{\mp}S_{SC}^{tt} - S_{SC}^{\phi t}}{\Omega_+ - \Omega_-}. \tag{101}$$

It is important to note that the components of the SEMT here are given in the spacetime coordinates (SC) i.e,

$$S_{SC}^{\mu\nu} = e_a{}^{\mu}e_b{}^{\nu}\gamma^{ac}\gamma^{bd}S_{cd}, \tag{102}$$

where S_{cd} is given by Eq.(82). Explicitly, we have

$$\begin{aligned}
S_{SC}^{tt} &= \frac{A^2f^4(A^2S_{tt} - 2AS_{t\phi} + S_{\phi\phi}) - 2\rho^2Af^2(S_{tt}A - S_{t\phi}) + \rho^4S_{tt}}{\rho^4f^2}, \\
S_{SC}^{t\phi} &= \frac{A\rho^2S_{tt} + 2A^2f^2S_{t\phi} - A^3f^2S_{tt} - Af^2S_{\phi\phi} - \rho^2S_{t\phi}}{\rho^4}, \\
S_{SC}^{\phi\phi} &= \frac{f^2(A^2S_{tt} - 2AS_{t\phi} + S_{\phi\phi})}{\rho^4}.
\end{aligned} \tag{103}$$

The angular velocities of the geodesic streams are shown in figure 13.

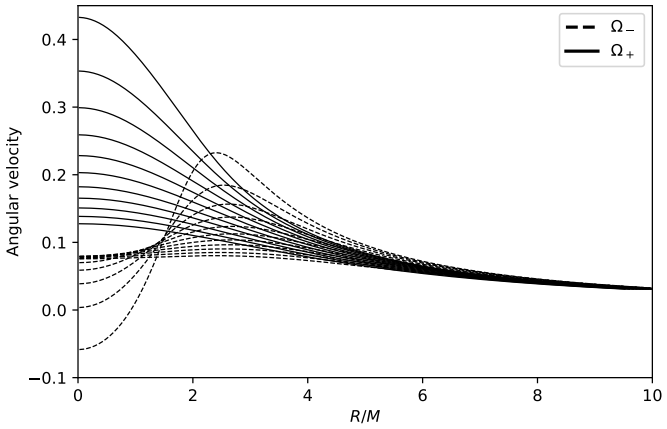

Figure 13: The angular velocity $\Omega_{\pm}$of the matter-streams. They correspond to the disks for constant $b = [0.613, 0.87, 1.11, 1.34, 1.56, 1.78, 2.00, 2.21, 2.42, 2.63, 2.84]$. Only one ergoregion-producing disk is shown.

With an increasing proper circumferential radius, the prograde (Ω_+) stream decreases slightly for all disks. The retrograde (Ω_-) stream exhibit a decrease in angular velocity up to $R/M \approx 1.5$ after which it increases with a peak at $R/M \approx 2.4$, and subsequently starts to drop again, converging with the prograde stream. The prograde stream never obtains a zero angular velocity, and both of the streams converge at $\Omega_+ \approx \Omega_- \approx 0.1$.

The densities of the streams in this configuration are shown in figure 14, and the sum of their densities in figure 15.

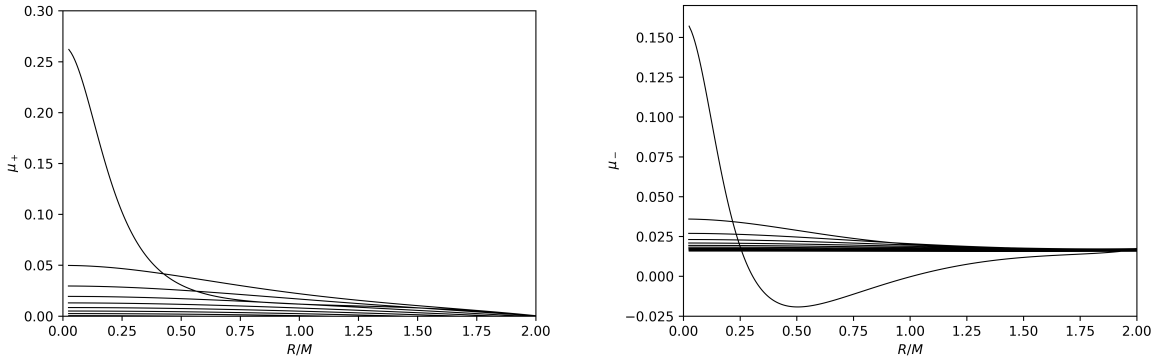

Figure 14: The densities $\mu_\pm$ for $b = [0.613, 0.87, 1.11, 1.34, 1.56, 1.78, 2.00, 2.21, 2.42, 2.63, 2.84]$.

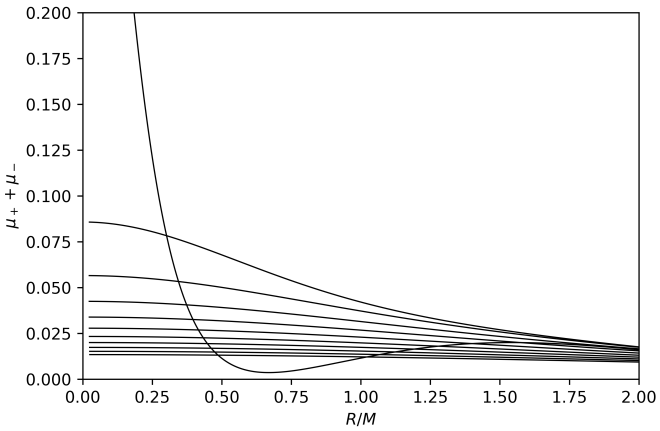

Figure 15: The sum of the stream's densities are positive everywhere.

In figure 15, we find that the WEC is satisfied for the SEMT, but as seen in figure 14, the retrograde stream itself does not, suggesting that the CRGS model is a non-physical consideration. The ergoregion-producing disk $b = 0.613$ has a defined density at $R/M = 0$, but is not shown in figure 15 for visibility.

7 Gravitational collapse

Apart from examining the properties of static disks, one of the main goals of this thesis is to consider a surface that is changing with time. Such a disk would collapse in on itself in the ρ- and z direction until all of the matter in the source is confined to a point. Since ρ and z depends on time t and s, we find that, during the surface evolution, the basis vectors have the same form as given in Eq.(68). The case can be readily visualized in figure 16.

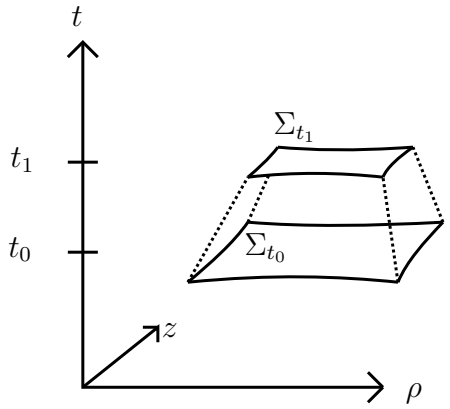

Figure 16: An illustration of the disk undergoing collapse in time. The illustration exhibits the surface at an initial time t_0 and a later time t_1.

A collapse may imply that the symmetries previously discussed for the static case are non-existent. In addition, the geodesics traveling alongside the surface may not stay there throughout the evolution of the disk but may leave it.

The SEMT constructed by the time-dependent basis vectors implies a 3×3 matrix, requiring three-component vectors to construct it. Even though the most realistic case concerns a decrease of proper circumferential radius and thickness in z, the expressions are too long to write out in this thesis. Therefore, another simplification will be made to draw some conclusions about gravitational collapse.

7.1 Constant surface s

Concerning gravitational collapse, only a collapse in the thickness of the disk, which is parameterized by z, will be considered. Furthermore, the thickness will not change with the radius from the center inside the surface. Therefore, we will impose upon the basis vectors: $z' = \dot{\rho} = 0$ and $\rho' = 1$. Hence

$$e_a{}^{\mu} = \begin{pmatrix} 1 & 0 & 0 & \dot{z} \\ 0 & 1 & 0 & 0 \\ 0 & 0 & 1 & 0 \end{pmatrix}, \; n_{\mu} = (-\lambda \dot{z}, 0, 0, \lambda), \; \lambda^2 = \frac{f h \, \rho^2}{h \, A^2 f^2 \dot{z}^2 - h \dot{z}^2 \rho^2 + \rho^2 f^2}. \tag{104}$$

These requirements imply the following extrinsic curvature

$$\begin{aligned}
K_{(t)(t)} &= \frac{\lambda\left(2hA\,f^3\left(A_z\right)\dot{z}^2+3h\left(f_z\right)\dot{z}^2\rho^2-f\left(h_z\right)\dot{z}^2\rho^2-2\ddot{z}fh\,\rho^2-f^2\left(f_z\right)\rho^2\right)}{2fh\,\rho^2},\\
K_{(t)(\phi)} &= \frac{\lambda\left(f\left(h\left(f^2A^2+\rho^2\right)\dot{z}^2-\rho^2f^2\right)\left(A_z\right)+2\rho^2A\left(f_z\right)\left(h\dot{z}^2-\frac{f^2}{2}\right)\right)}{2f\,\rho^2h},\\
K_{(t)(s)} &= \frac{\lambda\left(-f\left(h_\rho\right)\rho^2+h\left(f^3A\left(A_\rho\right)+2\rho^2\left(f_\rho\right)\right)\right)\dot{z}}{2f\,\rho^2h},\\
K_{(\phi)(\phi)} &= -\frac{\lambda\left(\left(f^2A^2+\rho^2\right)\left(f_z\right)+2f^3A\left(A_z\right)\right)}{2fh},\\
K_{(\phi)(s)} &= \frac{\dot{z}\left(\left(A^2f^3+\rho^2f\right)\left(A_\rho\right)+2A\rho\left(\left(f_\rho\right)\rho-f\right)\right)\lambda}{2f\,\rho^2},\\
K_{(s)(s)} &= -\frac{\lambda\left(h\left(f_z\right)-\left(h_z\right)f\right)}{2fh}.
\end{aligned} \tag{105}$$

The trace of the extrinsic curvature will be time-dependent, suggesting that a family of geodesics intersecting the surface will change with time as well. However, the trace (along with the SEMT) are still too long to explicitly state.

However, it would be interesting to see how the collapse looks initially when the surface evolution is very slow. Of course, this only applies to a minimal time interval during the "start" of the collapse. To properly investigate the adiabatic behavior of the initial collapse, we will make an ansatz

$$z(t) = b - Qt, \tag{106}$$

where $0 < Q \ll 1$, so that we can neglect higher-order terms and second derivatives of $L(t)$. Furthermore, these assumptions will keep the induced metric unchanged from the CRGS case. This simplifies the extrinsic curvature and its trace significantly, relating to the static case, denoted by K^0_{ab} up to first order

$$K_{ab} = K^0_{ab} + K^1_{ab}, \tag{107}$$

in which K^1_{ab} is a symmetric correction matrix with the form

$$\begin{aligned}
K^1{}_{(t)(s)} &= -\frac{\lambda\left(hA\,f^3\left(A_\rho\right)+2h\left(f_\rho\right)\rho^2-f\left(h_\rho\right)\rho^2\right)}{2fh\,\rho^2}Q,\\
K^1{}_{(\phi)(s)} &= -\frac{\lambda\left(A^2f^3\left(A_\rho\right)+2A\left(f_\rho\right)\rho^2+f\left(A_\rho\right)\rho^2-2Af\rho\right)}{2f\,\rho^2}Q,
\end{aligned} \tag{108}$$

with all other components being zero. The trace will only contain second-order correction terms, so

$$K^a{}_a = K^{0a}{}_a. \tag{109}$$

As can be seen in the extrinsic curvature, this adiabatic evolution suggests time independence. The SEMT can be similarly described with a correction matrix while still being

static - only perturbed to allow initial evolution

$$S_{ab} = S^0_{ab} + S^1_{ab}. \tag{110}$$

The time independence suggests that the vectors in the surface are also time-independent. Therefore the vectors that admit a vector-decomposition are only dependent on ρ. However, now the SEMT has a slightly more complicated form with nonzero components in the $s-$direction

$$S_{ab} = S^0_{ab} + S^1_{ab} = \begin{pmatrix} S_{tt} & S_{t\phi} & S_{ts} \\ S_{t\phi} & S_{\phi\phi} & S_{\phi s} \\ S_{ts} & S_{\phi s} & 0 \end{pmatrix}. \tag{111}$$

Like the static case, one can either diagonalize S_{ab} or use the geodesic equations to find the density, pressure, and vector components. In the following, we will first utilize the geodesic equations.

7.2 Geodesic streams around a perturbed disk

Since the SEMT in Eq.(111) contains a small correction in the s-components, we assume that all that is required are the vectors found in the previous cases (which builds up the $S_{tt}, S_{t\phi}$ and $S_{\phi\phi}$ parts) plus a correction vector $Z^\mu = (v_1, v_2, v_3, 0)$, where v_1, v_2 and v_3 are small correction functions (in Q) dependent on ρ. They are here assumed to be time-independent since their time-dependent part is proportional to Q^2. Therefore the new vector of interest has the form

$$U^\mu = (N_\pm + Qv_1, N_\pm\Omega_\pm + Qv_2, Qv_3, -\dot{z}N_\pm), \tag{112}$$

In which the last component is nonzero as a consequence of the new perturbed vector basis. Note that we require $v_3 \neq 0$ to be able to decompose S_{ab} in a way that is consistent with a small correction vector; i.e. $U^\alpha Z^\rho \neq 0$.

Even though the unperturbed U^a itself satisfies the geodesic equations, this new perturbed vector might not. This is because the geodesic equations are highly non-linear. Using the same symmetry arguments as before, we notice that the $z-$component of the geodesic equations is odd in z, so the averaged Christoffel symbols cancel in $\Gamma^z{}_{\alpha\beta}U^\alpha U^\beta = 0$, where $U^\mu \to U^\mu_0 + Z^\mu$. This observation means that we only need to solve the first three geodesic equations, which are:

$$\begin{aligned} &\alpha_1 v_3 = 0 \\ &\alpha_2 v_3 = 0 \\ &\alpha_3 v_1 + \alpha_4 v_2 + \alpha_5 = 0, \end{aligned} \tag{113}$$

in which α_i are functions of ρ and are too long to write out. The system tells us that v_3 is determined by the first and second equation only. If $v_3 \neq 0$ then both α_1 and α_2 have to be zero. First, we note that

$$\frac{\partial N_\pm}{\partial \rho} = N^3_\pm P\Omega_{,\rho}, \tag{114}$$

where $P = g_{\phi\phi}\Omega + g_{t\phi}$. The derivation of this expression is given in the appendix. For both α_1 and α_2 to be zero, then the following must also be fulfilled

$$\chi = \beta_1 \frac{\partial A}{\partial \rho} + \beta_2 \frac{\partial f}{\partial \rho} - \beta_3 = 0, \tag{115}$$

in which

$$\begin{aligned}
\beta_1 &= f\left(\left(\Omega_\pm A + 1\right)\left(\left(\Omega_\pm P + 1\right)A + P\right) f^2 + \Omega_\pm \rho^2 \left(\Omega_\pm P + 1\right)\right), \\
\beta_2 &= 2\rho^2 \left(P\,\Omega_\pm^2 + \Omega_\pm\right) A + \Omega_\pm P + \frac{1}{2}, \\
\beta_3 &= 2\rho\Omega_\pm f\left(P\Omega_\pm A + P + A\right).
\end{aligned} \tag{116}$$

The value of χ is shown in figure 17.

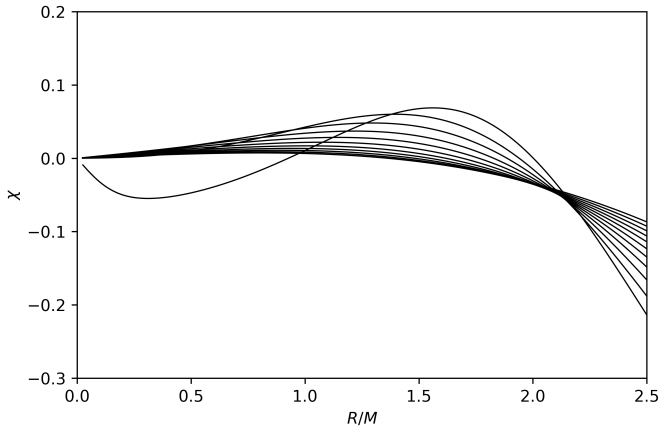

Figure 17: The value of χ as plotted for the eleven disks for visibility. It has a zero-value at specific points unique to each disk. There are two points at which a nonzero correction value v_3 can be obtained.

Figure 17 is just a statement of the difference between $\Omega_{,\rho}$, given by $\alpha_1 - \alpha_2 = 0$. Therefore, Eq.(115) might be satisfied even though α_1 and α_2 are nonzero if $\alpha_1 = \alpha_2$. There exist one more condition to look at: if $\alpha_1 = 0$, then we have

$$\Omega_{,\rho} = -\frac{f^3 A^2 \Omega\left(A_\rho\right) + f^3 A\left(A_\rho\right) + \Omega\left(A_\rho\right)\rho^2 f + 2A\Omega\left(f_\rho\right)\rho^2 - 2A\Omega\rho f + \rho^2\left(f_\rho\right)}{fP\,\rho^2}. \tag{117}$$

From figure 13, we find that the derivative of the angular velocity of the prograde stream must decrease as we move further away from the center. Therefore we require

$$\Lambda := \frac{f^3 A^2 \Omega_+\left(A_\rho\right) + f^3 A\left(A_\rho\right) + \Omega_+\left(A_\rho\right)\rho^2 f + 2A\Omega_+\left(f_\rho\right)\rho^2 - 2A\Omega_+\rho f + \rho^2\left(f_\rho\right)}{fP\,\rho^2} \geq 0 \tag{118}$$

In fact, as seen in figure 18, the inequalities are satisfied.

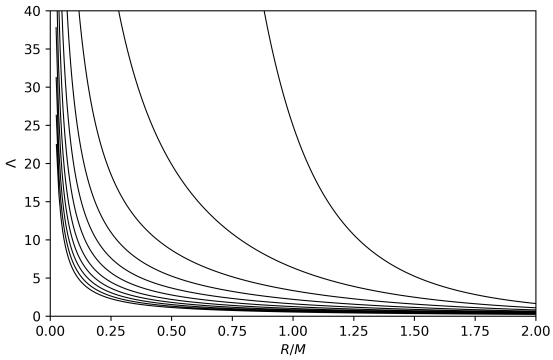

Figure 18: The derivative of the angular velocity is negative for all values of proper circumferential radius. It goes to zero for large R/M, in agreement with the converging velocity for the geodesics. A singularity is present at $R/M = 0$, in disagreement with the finite velocity in figure 13.

We can see that the derivative is undefined for $R/M = 0$, which disagrees with the results plotted in figure 13, where the curves are well-defined for all values of proper circumferential radius.

The derivative of angular velocity and $v_3 \neq 0$ only hold for specific values of R/M, implying that geodesic streams as a source of the perturbed disk do not represent a physical configuration. If v_3 is taken to be zero, it follows that $v_1 = v_2 = 0$ as well, which fails to represent the SEMT. If higher-order terms are included, the geodesic equations admit solutions, but then the SEMT cannot be represented by our ansatz to first order.

However, as in the static case, a diagonalization may be performed to get angular velocities that do not satisfy the geodesic equations. In this case, we choose the correction vector to have the form $Z^\mu = (0, 0, v_3, 0)$ such that

$$\begin{aligned} U^\mu_\pm &= (N_\pm, N_\pm\Omega_\pm, 0, -v_3 N_\pm), \\ U^\mu &= U^\mu_\pm + Z^\mu = (N_\pm, N_\pm\Omega_\pm, v_3, -v_3 N_\pm). \end{aligned} \tag{119}$$

Hence we need to find $N_\pm$, $\Omega_\pm$ and Q such that the following equation is satisfied

$$S^{\mu\nu} = \mu_+ \left[U^\mu_+ U^\nu_+ + \frac{1}{2}\left(U^\mu_+ Z^\nu + U^\nu_+ Z^\mu \right) \right] + \mu_- \left[U^\mu_- U^\nu_- + \frac{1}{2}\left(U^\mu_- Z^\nu + U^\nu_- Z^\mu \right) \right]. \tag{120}$$

Since we require the normalization condition, we find (and perform an approximation of $Q = 0$ up to first order)

$$N^2_\pm = -\frac{1}{g_{\phi\phi}\Omega^2_\pm + 2g_{t\phi}\Omega_\pm + g_{tt}}, \tag{121}$$

which is the same condition as before. However, diagonalization of the SEMT leads to complex values of v_3, implying that this is not a physical consideration.

8 Conclusion and discussion

We used a formalism to adequately explain physical quantities confined to a subset of a spacetime corresponding to a surface. This was done to see what kind of sources there exists that produces the Kerr metric. We find that the thin-shell formalism can be applied to track particles (and hence the behavior of the surface as a whole) through time to see how natural sources would behave when observed from an LNRF- or $\phi-$isotropic frame.

We utilized a perfect fluid approach in section 6.1 by diagonalizing the energy-momentum tensor. This was done to see how matter would behave as a source to the Kerr metric. The velocities were finite along with a positive density and pressure, effectively satisfying all energy conditions. The trajectories of the streams were not assumed to follow geodesics and may therefore not represent a natural source, so values of the thickness b had to be chosen carefully such that the pressure and density remain positive for all distances away from the center. We presented twelve cases for different values of b, of which two could produce ergoregions. No angular velocity was found to approach the speed of light.

The CRGS model was investigated in section 6.2, where the source was found to be formed by counter-rotating streams of matter that obey the geodesic equations. Since the streams follow geodesics, their densities must be positive. Now, however, the angular velocities differ in sign, so the two streams contain different densities. It was found that the retrograde stream in the ergoregion-producing disk had a negative energy density at $R/M \approx 0.5$, violating the WEC and DEC. Together, however, they satisfied the WEC and DEC, as expected from Einstein's field equations. The angular velocity was well-defined for all values of circumferential radius. The prograde stream attained its maximum close at the horizon, while the retrograde stream peaked at $R/M \approx 2.4$.

An adiabatic gravitational collapse was investigated in section 7, for which we concluded that no geodesic motion was possible up to first order. A vector basis constructed from a decreasing z will cause a z-motion onto the trajectories. The geodesic equations for small perturbations to the surface energy-momentum tensor implied contradicting results, forcing the correction vector to be the null vector. Hence a small perturbation in the first order was concluded to be impossible.

Like the static case, a diagonalization can be performed to construct collapsing streams of matter that do not satisfy the geodesic equations. The correction term v_3 was found to be complex due to the normalization condition for the vectors. In the case where $N_+ = N_-$, the constant is entirely real, but then the densities are infinite everywhere. So we conclude that neither geodesic treatment of a perturbation to the disks nor diagonalization is a viable approach up to first order.

However, a less restrictive ansatz $z \to z(\rho)$ could be made, in which case more degrees of freedom would be available in the geodesic equations. This would not restrict v_3 as tightly, possibly allowing solutions to the geodesic equations where $v_3 \neq 0$.

Appendix

Variation of the Christoffel symbols

To show that the variation of the Christoffel symbols transforms like a tensor, we can examine the covariant derivative of the variation of the metric

$$\nabla_\lambda(\delta g_{\mu\nu}) = \delta(\nabla_\lambda g_{\mu\nu}) + g_{\rho\nu}\delta\Gamma^\rho{}_{\mu\lambda} + g_{\mu\rho}\delta\Gamma^\rho{}_{\lambda\nu}. \tag{A1}$$

However, the connection (defined by the Christoffel symbols) comes from the choice that the covariant derivative of the metric tensor is zero. Hence we obtain

$$\nabla_\lambda(\delta g_{\mu\nu}) = g_{\rho\nu}\delta\Gamma^\rho{}_{\mu\lambda} + g_{\mu\rho}\delta\Gamma^\rho{}_{\lambda\nu}. \tag{A2}$$

The task at hand is to show that the variation of the Christoffel symbol is a tensorial quantity, so it has to be isolated and expressed in terms of the covariant derivatives. There exists a helpful trick, where we can permute the indices threefold such that we obtain a system of three equations [19]

$$\begin{aligned}
\nabla_\lambda(\delta g_{\mu\nu}) &= g_{\rho\nu}\delta\Gamma^\rho{}_{\mu\lambda} + g_{\mu\rho}\delta\Gamma^\rho{}_{\lambda\nu} \\
\nabla_\nu(\delta g_{\lambda\mu}) &= g_{\rho\lambda}\delta\Gamma^\rho{}_{\nu\mu} + g_{\nu\rho}\delta\Gamma^\rho{}_{\mu\lambda} \\
\nabla_\mu(\delta g_{\nu\lambda}) &= g_{\rho\mu}\delta\Gamma^\rho{}_{\lambda\nu} + g_{\lambda\rho}\delta\Gamma^\rho{}_{\nu\mu}.
\end{aligned} \tag{A3}$$

Adding the third and second equations and subtracting the first yields

$$\nabla_\mu(\delta g_{\nu\lambda}) + \nabla_\nu(\delta g_{\lambda\mu}) - \nabla_\lambda(\delta g_{\mu\nu}) = 2g_{\rho\lambda}\delta\Gamma^\rho{}_{\nu\mu}. \tag{A4}$$

Using the relation $g^{\mu\nu}g_{\nu\rho} = \delta^\mu{}_\rho$, Eq.(A4) gives

$$\delta\Gamma^\rho{}_{\nu\mu} = \frac{1}{2}g^{\rho\lambda}\left(\nabla_\mu(\delta g_{\nu\lambda}) + \nabla_\nu(\delta g_{\lambda\mu}) - \nabla_\lambda(\delta g_{\mu\nu})\right), \tag{A5}$$

which is a tensorial quantity since each term contains covariant derivatives of the variation of the metric tensor.

Geodesic equation for non-collapsing geodesic streams

We want to evaluate the geodesic equation

$$U^\alpha_\pm U^\mu_{\pm;\alpha} = 0. \tag{A6}$$

Since the particle stays on the surface when transported along a geodesic, we can decompose the geodesic equation in Eq.(A6)

$$e^a{}_\mu U^\alpha_\pm U^\mu_{\pm;\alpha} = 0. \tag{A7}$$

The only equation that is not automatically solved is the ρ-component

$$e^a{}_\rho U^\alpha_\pm \partial_\alpha U^\rho_\pm - e^a{}_\mu \Gamma^\mu{}_{\alpha\beta} U^\alpha_\pm U^\beta_\pm = 0. \tag{A8}$$

Since $U^\mu_\pm = (N_\pm, N_\pm \Omega_\pm, 0, 0)$, we find that the first term vanishes so

$$\Gamma^t{}_{\alpha\beta} U^\alpha_\pm U^\beta_\pm + \Gamma^\phi{}_{\alpha\beta} U^\alpha_\pm U^\beta_\pm + \Gamma^\rho{}_{\alpha\beta} U^\alpha_\pm U^\beta_\pm = 0. \tag{A9}$$

The Christoffel symbols $\Gamma^t{}_{\mu\nu}$ and $\Gamma^\phi{}_{\mu\nu}$ are only nonzero for components with either μ or ν being equal to ρ or z, for which the vector elements are zero. The only surviving term is therefore $\Gamma^\rho{}_{\mu\nu}$ with the nonzero components

$$\begin{aligned}
\Gamma^\rho{}_{tt} &= \frac{f}{2h}\frac{\partial f}{\partial \rho}, \\
\Gamma^\rho{}_{t\phi} &= \frac{f}{2h}\left(A\frac{\partial f}{\partial \rho} + f\frac{\partial A}{\partial \rho}\right), \\
\Gamma^\rho{}_{\phi\phi} &= \frac{1}{2fh}\left(\frac{\partial f}{\partial \rho}\left(A^2 f^2 + \rho^2\right) + 2f^3 A\frac{\partial A}{\partial \rho} - 2\rho f\right).
\end{aligned} \tag{A10}$$

Substituting the results in Eq.(A10) into Eq.(A9) we obtain

$$\frac{\partial f}{\partial \rho}\left[(A\Omega_\pm + 1)^2 f^2 + \rho^2 \Omega_\pm^2\right] - 2f\Omega_\pm\left[\rho\Omega_\pm - f^2\frac{\partial A}{\partial \rho}(A\Omega_\pm + 1)\right] = 0. \tag{A11}$$

The derivative of the normalization constant

If we restric ourselves to the N_+ case such that $N_+ \to N, \Omega_+ \to \Omega$, then the normalization constant squared N^2 is expressed as

$$N^2 = -\frac{1}{g_{\phi\phi}\Omega^2 + 2g_{t\phi}\Omega + g_{tt}}. \tag{A12}$$

Taking the derivative with respect to ρ gives

$$\frac{dN^2}{d\rho} = 2N\frac{dN}{d\rho} = N^4\left(g_{\phi\phi,\rho}\Omega^2 + 2g_{t\phi,\rho}\Omega + g_{tt,\rho} + 2g_{\phi\phi}\Omega\Omega_{,\rho} + 2g_{t\phi}\Omega_{,\rho}\right). \tag{A13}$$

However, the first three terms in the brackets are equal to zero through the geodesic equations. Hence

$$\frac{dN}{d\rho} = N^3(g_{\phi\phi} + g_{t\phi})\Omega_{,\rho} = N^3 P\Omega_{,\rho}. \tag{A14}$$

References

[1] A. Einstein, *Relativity: the special and the general theory*. General Press, 2016.

[2] K. Schwarzschild, "Über das gravitationsfeld eines massenpunktes nach der einsteinschen theorie," *Sitzungsberichte der Königlich Preußischen Akademie der Wissenschaften (Berlin*, pp. 189–196, 1916.

[3] J. R. Oppenheimer and H. Snyder, "On continued gravitational contraction," *Physical Review*, vol. 56, no. 5, p. 455, 1939.

[4] R. P. Kerr, "Gravitational field of a spinning mass as an example of algebraically special metrics," *Physical review letters*, vol. 11, no. 5, p. 237, 1963.

[5] K. S. Thorne, C. W. Misner, and J. A. Wheeler, *Gravitation*. Freeman, 2000.

[6] R. Penrose and R. Floyd, "Extraction of rotational energy from a black hole," *Nature Physical Science*, vol. 229, no. 6, pp. 177–179, 1971.

[7] H. D. Wahlquist, "Interior solution for a finite rotating body of perfect fluid," *Physical Review*, vol. 172, no. 5, p. 1291, 1968.

[8] J. Bičák and T. Ledvinka, "Relativistic disks as sources of the kerr metric," *Physical review letters*, vol. 71, no. 11, p. 1669, 1993.

[9] T. Ledvinka and J. Bičák, "Disk sources of the kerr and tomimatsu-sato spacetimes: construction and physical properties," *Physical Review D*, vol. 99, no. 6, p. 064046, 2019.

[10] C. Barrabes and W. Israel, "Thin shells in general relativity and cosmology: The lightlike limit," *Physical Review D*, vol. 43, no. 4, p. 1129, 1991.

[11] A. Einstein, "Riemann-geometrie mit aufrechterhaltung des begriffes des fernparallelismus," *Albert Einstein: Akademie-Vorträge: Sitzungsberichte der Preußischen Akademie der Wissenschaften 1914–1932*, pp. 316–321, 2005.

[12] H. Weyl, "Elektron und gravitation. i," *Zeitschrift für Physik*, vol. 56, no. 5-6, pp. 330–352, 1929.

[13] R. H. Boyer and R. W. Lindquist, "Maximal analytic extension of the kerr metric," *Journal of mathematical physics*, vol. 8, no. 2, pp. 265–281, 1967.

[14] H. Weyl, "Zur gravitationstheorie," *Annalen der Physik*, vol. 359, no. 18, pp. 117–145, 1917.

[15] T. Lewis, "Some special solutions of the equations of axially symmetric gravitational fields," *Proceedings of the Royal Society of London. Series A, Containing Papers of a Mathematical and Physical Character*, vol. 136, no. 829, pp. 176–192, 1932.

[16] A. Papapetrou, "A static solution of the equations of the gravitational field for an arbitary charge-distribution," in *Proceedings of the Royal Irish Academy. Section A: Mathematical and Physical Sciences*, vol. 51, pp. 191–204, JSTOR, 1945.

[17] E. Poisson, *A relativist's toolkit: the mathematics of black-hole mechanics*. Cambridge university press, 2004.

[18] S. W. Hawking and G. F. R. Ellis, *The large scale structure of space-time*, vol. 1. Cambridge university press, 1973.

[19] S. M. Carroll, *Spacetime and geometry*. Cambridge University Press, 2019.